

A High Torque Variable Stiffness Mechanism for the 'VSDD': Conceptual Design, Realization and Experimental Validation

J.S.T. (Jonas) Strecke

BSc Assignment

Committee:

Dr. R. Carloni

Dr.ir. M. Fumagalli

Prof.dr.ir. A. de Boer

Juli 2014

Report nr. 009RAM2014
Robotics and Mechatronics
EE-Math-CS
University of Twente
P.O. Box 217
7500 AE Enschede
The Netherlands

Contents

Acknowledgments	ix
Abstract	xi
1 Introduction	1
2 Evaluation of Variable Stiffness Concepts	3
2.1 Compliant Joints	3
2.1.1 'Physical Properties of a Spring'	4
2.1.2 'Changing Transmission between Load and Spring'	4
2.1.3 'Spring Preload'	5
2.2 Preliminary Evaluation	6
2.3 Possible Implementation and Choice of Design	8
3 Modelling	11
3.1 Analysis of Variable Stiffness Mechanism	11
3.1.1 Torque-Deflection Characteristics	11
3.1.2 Torque-Deflection Plots	13
3.1.3 Force Approach	15
3.1.4 Apparent Output Stiffness	16
3.2 Motoranalysis	17
3.2.1 PowerAnalysis	17
3.2.2 Transmission Analysis	18
3.2.3 Volume Analysis	21
3.2.4 Choice of Motor and Gear Combination	23
4 Design	25
4.1 Variable Stiffness Mechanism	25
4.2 Motor and Gear Module	27
4.3 Datasheet	29

5	Proof of Concept	31
5.1	Adaptation of Design/Rapid Prototyping	31
5.2	Test and Results	33
6	Discussion	35
7	Conclusion and Future Work	37
7.1	Conclusion	37
7.2	Future Work	37
A		39
A.1	Calculation of Leaf Spring	39
A.2	Calculation of Pivot Point Dimension for Lever Arm Mechanism . .	39
A.3	MATLAB	40
B		45
	References	49

List of Figures

1.1	Simplified 2D representation of the Differential Drive including its Joint Motors and the Variable Stiffness Mechanism (VSM).	2
2.1	Jack Spring Actuator with active and inactive coil regions and principle of changing stiffness by rotation of spindle.	4
2.2	Principle of Lever Arm Mechanism	4
2.3	Principle of VS Joint: Roller in equilibrium position with zero stiffness on the left hand side. Actuator Force F_A has to be applied to increase the stiffness by pretensioning the springs. On the right of the figure the joint is deflected by φ	5
2.4	Principle of FSJ: a) shows the FSJ in equilibrium position and stiffness preset $\phi_0 = 0$. The Springs are attached to the camdisks, can move in horizontal direction however. In b) the camdisks were rotated respectively to each other by ϕ_{stiff} and the spring is expanded, so that the joint is in a stiff state. A deflection of the joint occurs when the rollers are moved out of their equilibrium position by φ in c) with an arbitrary stiffness preset of ϕ_1	5
2.5	Adaptation of the 'Jack Spring' towards use in the Differential Drive.	8
2.6	Eq. Position of Jack Spring in DD	8
2.7	Deflection of Jack Spring in DD.	9
2.8	Adaptation of the Pretension Mechanism of 'DLR' towards use in the Differential Drive.	9
3.1	State of Spring as Function of Deflection φ on Cam disk.	11
3.2	Different Spring Setups	13
3.3	Torque-Deflection Plot for Different Spring Setups	14
3.4	Deflection Range	14
3.5	Force representation of the VSM mechanism.	15
3.6	Output Stiffness for different stiffness presets, starting with $\phi = 0^\circ$, so very compliant and ending with a stiff preset of $\phi = 20^\circ$	16
3.7	2D-View of the Assembly without Motor, all dimensions in mm.	21

4.1	Overview of Design of Variable Stiffness Mechanism	25
4.2	More Detailed View of Design	26
4.3	Exact Measurements of the Spring Space for Extreme Cases.	26
4.4	Variable Stiffness Joint including Motor, Gear and Clutch System.	27
4.5	Labeled Section View of Variable Stiffness Joint in a) and the friction clutch integrated into the Variable Stiffness Joint in b)	28
5.1	SOLIDWORKS Model of Test Setup	31
5.2	Deflection vs Output Torque for Springs used in Test Setup	32
5.3	Fully Assembled Test Setup with F/T Sensor(right) and Magnetic Encoder(left).	33
5.4	Deflection vs Output Torque obtained by testing	34
6.1	Compensated Deflection vs Output Torque Plot. The expected plots are depicted in black colour.	36
A.1	Torque-Deflection MATLAB file for different Spring Setups, Page 1.	40
A.2	Torque-Deflection MATLAB file for different Spring Setups, Page 2.	41
A.3	Torque-Deflection MATLAB file for different Spring Setups, Page 3.	41
A.4	Zoom into fig.3.4:Output torque at a deflection of 25°	41
A.5	Plots of force approach and approach based on [15]. Plotted with a deflection range of $\phi = [-25^\circ \ 25^\circ]$ and $\phi = 0^\circ$. τ_{10} and τ_{cup} is the torque produced by the springs on the upper cam profile. τ_{20} and τ_{cdown} is the torque produced by the springs on the lower cam profile.	42
A.6	Torque-Deflection MATLAB file for fundamental approach comparison, Page 1.	42
A.7	Torque-Deflection MATLAB file for fundamental approach comparison, Page 2.	43
A.8	Torque-Deflection MATLAB file for fundamental approach comparison, Page 3.	43
A.9	Setup for the measurement of the Spring constant k including Newton-meter, weights(below) and scale.	44
A.10	Plot of Measured Spring Deflection vs Measured Force. The Data was evaluated using Matlab Curve Fitting with $F = kx$ and resulted in $k = 0.7401 [N/mm]$	44
B.1	Characteristic data of TQ Drive ILM25x08.	45
B.2	Characteristic Data of TQ Drive ILM38x06.	46
B.3	Characteristic Data of TQ Drive ILM38x12.	46
B.4	Characteristic Data of TQ Drive ILM50x08.	47

List of Tables

2.1	Evaluation of different VS-Mechanisms based on compactness and robustness.	6
3.1	Values for input torque τ_{in} and gear ratio r with $\eta = 0.85$	19
3.2	Values for input torque τ_{in} and gear ratio r with $\eta = 0.3$	19
3.3	Values for gear ratio r with $\eta = 0.85$ divided by r_{HD}	20
3.4	Values for gear ratio r with $\eta = 0.3$ divided by r_{HD}	20
3.5	Gear ratio r based on $\tau_{nom_{in}}$ and τ_{avg} for additional motor models . .	20
3.6	Possible Arrangements of Motor. Upper horizontal column displays the placement of the motor in radial or axial position to the VS-mechanism. left Vertical row displays the shaft alignment of the VS-Mechanism as either parallel or perpendicular.	21
3.7	Possible gear and non-back-drivable element addition to previous motor arrangements.	22
4.1	Incomplete Datasheet of VSM Design	29

Acknowledgments

First of all I would like to thank my supervisors Matteo Fumagalli and Raffaella Carloni for their support and advise throughout the course of my Bachelors Project. Special thanks go to Éamon Barrett, who helped me with his expertise and was always available to have a vivid discussion with. I consider him to be my second daily supervisor.

The patience of my roommates of Jottir Weidenaar and Mateo Soejenbos through my ups and downs in the last year has been amazing and i am thankful they were always there for me. A very special person, that gave me confidence and did not stop believing in me is my girlfriend Merle Einhaus. You make me happy. Finally, i would like to mention my parents Magdalena and Dietmar Strecke. I owe them a great deal for how i think and act as a person. Their stubbornness for example, which i also inherited has made me able to face challenges in life and be able to go through rough times.

Abstract

In this study a variable stiffness mechanism with high torque output characteristics was developed for a differential drive. In doing so, different existing mechanisms and their underlying principles were investigated to elaborate further on a chosen design implementation. Based on this choice, the principle is modelled and realized according to the requirements imposed by the differential drive. Finally, validation of the model is achieved by tests of a simplified prototype.

The Outcome of this work forms a possible solution to the problem statement of a high torque variable stiffness mechanism, but has to be processed further to be fully integrated into the differential drive.

Chapter 1

Introduction

The performance of robotic arms has been improving over the past years significantly. A broader performance necessity has become indispensable due to the adaptation of robotic systems into subjects like medical application and manufacturing processes. Main objectives as a result of this adaptation and hence a closer human-robot interaction gives rise to criteria, like 'Interaction Safety' or 'Shock Robustness', as stated in [1]. On top of that autonomous robotics are generally in need of better physical interaction to avoid damage and manage tasks in an efficient and more adaptable manner. These criteria and demands paved the path towards an innovation of Variable Stiffness Actuators (VSA), which can adjust the compliance of a joint based on which task it has to perform.

Also the European 'SHERPA' project [2] develops a platform of aerial and ground robots collaborating closely with a human in rescue missions. Subsequently the robots have to be especially safe and adaptable due to the working conditions in a hostile environment. The 'Robotics and Mechatronics' Group of the 'University of Twente' is partaking in said project developing a robotic arm for the ground robot allowing it to execute tasks such as picking and placing of flying vehicles and interaction with obstacles of the unknown environment.

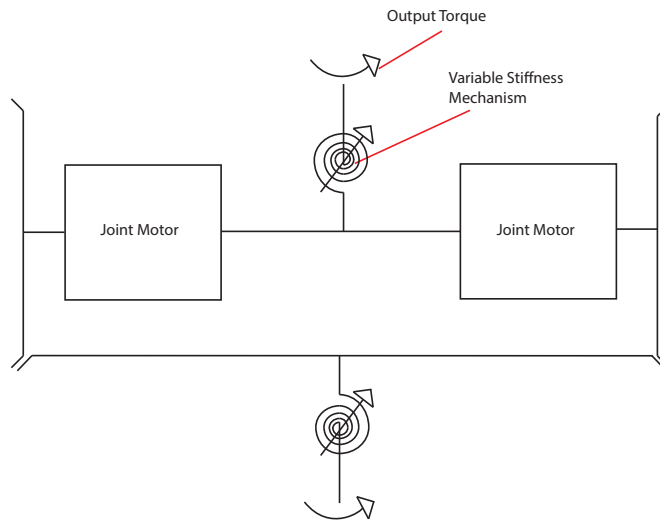


Figure 1.1: Simplified 2D representation of the Differential Drive including its Joint Motors and the Variable Stiffness Mechanism (VSM).

The 'Variable Stiffness Differential Drive (VSDD)' [3], was developed for the Shoulder joint of the ground rover in the 'SHERPA' project and enhances the compactness of the two DoF joint. A main objective when integrating a variable stiffness mechanism into the DD is to decouple the stiffness matrix from the transmission matrix to achieve independent control of position and compliance. A representation of the 'VSDD' is shown in figure 1.1. Due to the location in the shoulder, high torque characteristics but also a compact design are required of the VSA.

Chapter 2

Evaluation of Variable Stiffness Concepts

In Variable Stiffness Actuators a compliance adaptation and the control of equilibrium position is achieved by two motors. Variable stiffness mechanisms rely on three elementary principles to achieve a compliance adaptation according to [4], which alter the compliance based on 'Changing Transmission between Load and Spring', the 'Physical Properties of the Spring' and 'Spring Preload'.

In this chapter different mechanisms of each principle are evaluated according to their applicability to the differential drive. Requirements for the High-Torque VSM, like a maximum Output Torque of $\tau_{max} = 100[Nm]$ and dimensional restrictions of $100 \times 130[mm]$ (length and diameter of a cylinder, where the mechanism has to fit in) are the prime focus for this evaluation and form the goal of the research.

2.1 Compliant Joints

In [4] each of the above mentioned principles is described as follows. The idea of adopting the 'Physical Properties of a Spring' is to vary the parameters of the spring constant $k = \frac{EA}{L}$, with E as material modulus, A as cross-sectional area and L as effective beam length. The term 'Changing Transmission between Load and Spring' is self explicable, when having in mind that the stiffness can be adjusted in said manner. Stiffness adaptation by varying the pretension of a spring is categorized as 'Spring Preload'. A variety of compliant mechanisms have been developed for each of these stiffness variation concepts and a selection is listed in this chapter providing detailed explanation for each mechanism.

2.1.1 'Physical Properties of a Spring'

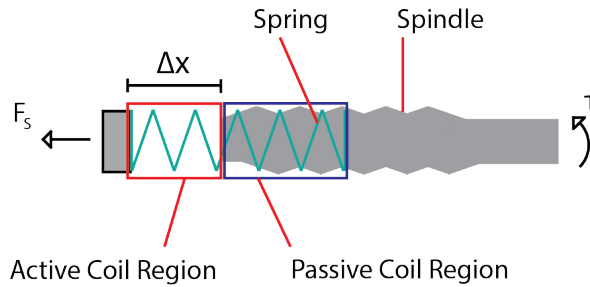


Figure 2.1: Jack Spring Actuator with active and inactive coil regions and principle of changing stiffness by rotation of spindle.

Jack Spring Actuator

The principle of the 'Jack Spring' Actuator [5] is to vary the effective length of a helical spring by adding or subtracting its coils. To do so, a rotating shaft divides the spring into active and inactive coil regions and thereby adjusts the spring force F_s (ref. fig. 2.1).

Leaf spring Mechanism

The 'Variable Stiffness Joint using Leaf Springs' [6] is another example of a variation of effective length of a spring to manipulate the stiffness and is a post-design of the 'Mechanical Impedance Adjuster' [7]. Instead of a common helical spring the joint implements four leaf springs. The stiffness of the leaf springs is adjusted by rollers, which can be considered pivot points moving on the leaf spring connected to the Output link.

2.1.2 'Changing Transmission between Load and Spring'

Lever Arm Mechanism

Actuators like the vsaUT-II [8], mVSA-UT [9], AwAS [10] and AwAS-II [11] realize a 'Changing Transmission between Load and Spring' by means of a lever arm mechanism.

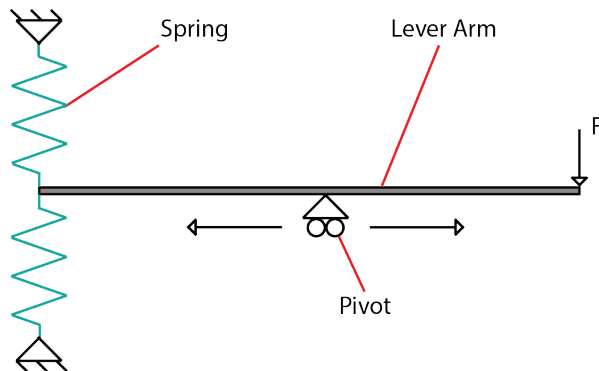


Figure 2.2: Principle of Lever Arm Mechanism

For the AwAS [10], springs are attached to a pivot point on the lever and can be moved along the lever arm. For the other three mentioned mechanisms, the length of the lever arm and thus the effect of the force on the spring can be changed by a moving pivot on the lever arm as illustrated in fig. 2.2, while the springs are attached to one end of the lever arm.

the force on the spring can be changed by a moving pivot on the lever arm as illustrated in fig. 2.2, while the springs are attached to one end of the lever arm.

2.1.3 'Spring Preload'

Pretension Mechanism

Adjusting the pretension of a spring by nonlinear profile manipulation is a typical example of 'Spring Preload' and is adopted by the 'VS-Joint' [12], the 'MACCEPA 2.0' [13] and the 'Floating Spring Joint (FSJ)' [14]. In fig. 2.3 the nonlinear profile of the spring of the 'VS-Joint' can be seen together with the spring attached to a roller. In order to change the stiffness the spring is compressed

by actuator force F_A , such that the applied torque has to be bigger to move the roller up the cam profile, when increasing stiffness. The 'MACCEPA 2.0' follows a similar approach, but makes use of a wire instead of rollers. The 'FSJ' is based on a similar principle illustrated in fig. 2.4. Here one spring is attached to two cam profiles with exponential shape, which press onto a pair of rollers. Deflection of the rollers, results in an

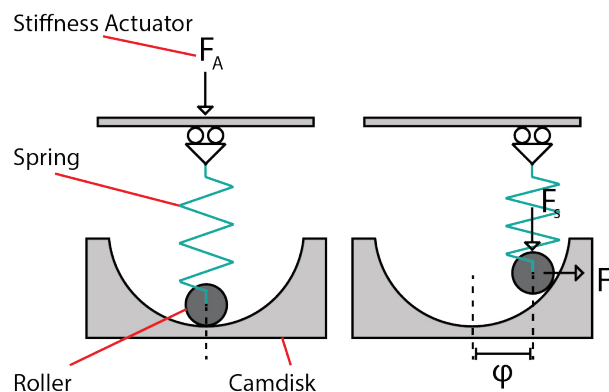


Figure 2.3: Principle of VS Joint: Roller in equilibrium position with zero stiffness on the left hand side. Actuator Force F_A has to be applied to increase the stiffness by pretensioning the springs. On the right of the figure the joint is deflected by ϕ .

expansion of the springs, because the rollers move up one of the two profiles. The compliance can be adjusted by actuating the cam profiles with respect to each other in opposite direction such that the spring is extended and more force is required to excite the rollers.

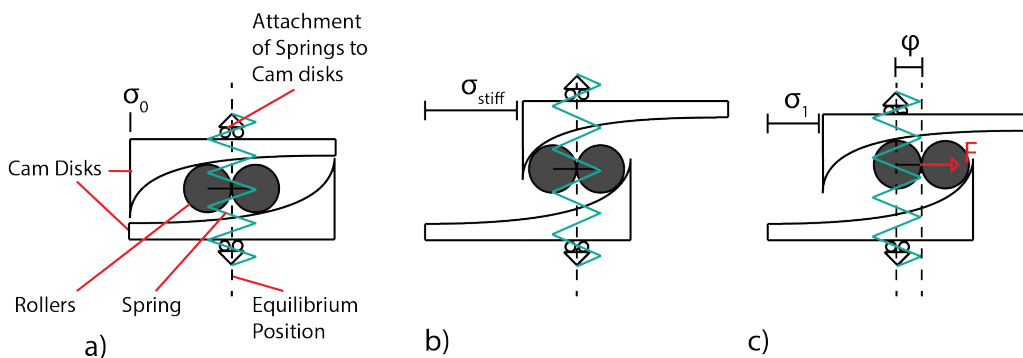


Figure 2.4: Principle of FSJ: a) shows the FSJ in equilibrium position and stiffness preset $\phi_0 = 0$. The Springs are attached to the camdisks, can move in horizontal direction however. In b) the camdisks were rotated respectively to each other by ϕ_{stiff} and the spring is expanded, so that the joint is in a stiff state. A deflection of the joint occurs when the rollers are moved out of their equilibrium position by ϕ in c) with an arbitrary stiffness preset of ϕ_1 .

2.2 Preliminary Evaluation

In this section advantages and disadvantages of each variable stiffness concept are discussed and evaluated according to the core requirements mentioned in the beginning of this chapter.

In all mechanisms the offset of compactness can be redirected to the size of the elastic element. This is because the spring element has to be able to produce a maximum deformation that resembles a total torque of $100[Nm]$. However, the 'Pretension Mechanism' of the 'MACCEPA 2.0' is not compact due to the pulley system. In the 'Leaf Spring Mechanism', the radius of the leaf springs was set to $40[mm]$ for the sake of space for housing or connections of the joint motors of the Differential Drive. The resulting calculation showed that for this leaf spring length and the defined output torque, the width of the leaf spring has a minimum value of $b = 29.63 [mm]$ (A.1), which has a negative influence on the compactness of this mechanism (see tab.2.1). The remaining principles, the 'Jack Spring', the 'Lever Arm Mechanism' and the 'Pretension Mechanism (VSJ,FSJ)' are evaluated based on the possible sizes of their springs. The 'VS-Joint' employs three springs, the 'FSJ' one big spring, the 'Jack Spring Actuator' one spring and the 'Lever Arm Mechanism' usually two. The 'Pretension Mechanism (VSJ,FSJ)' seems to be the most promising about the adaptation of multiple springs and usage of conventional springs, which influence the robustness and compactness positively (ref. 2.1). Another advantage is provided by its progressive torque deflection behavior, achieving high torques with high deflections.

The second factor, that needs to be evaluated is the torque requirement. A high output torque of the 'Jack spring' Mechanism and Preload Mechanism (MACCEPA 2.0) is unlikely or at the cost of compactness, because they implement only one spring. Next a closer look is taken at the 'Lever Arm Mechanism'. A FEM-Analysis for stresses acting on the pivot pin of the 'mVSA-UT' (shown in [9]) leads to doubt that the pivot in the lever arm mechanism can withstand high torques. However simple calculations were made in section A.2, that confute this.

	Pretension Mechanism (MACCEPA 2.0)	Leaf Spring Mechanism	Jack Spring Actuator	Lever Arm Mechanism	Pretension Mechanism (VSJ,FSJ)
Compact	-	-	+/-	+/-	+
Robust	-	+/-	-	+/-	+

Table 2.1: Evaluation of different VS-Mechanisms based on compactness and robustness.

Finally a choice had to be made to be further evaluated due to the adaptability of the principles in the differential drive in the next chapter. The 'Pretension Mechanism' is chosen to be assessed more in depth. According to the table, the 'Lever Arm Mechanism' should be chosen as a possible implementation alternative. However, a novel implementation for the 'Jack Spring' Actuator with two spring elements was thought of and will be compared to the integration of the 'Pretension Mechanism' into the DD.

2.3 Possible Implementation and Choice of Design

A tradeoff between the various mechanism specified previously was made to compare the possible implementation into the differential drive of two working principles. The 'Jack Spring Actuator' and Pretension Mechanism were chosen to be analyzed further.

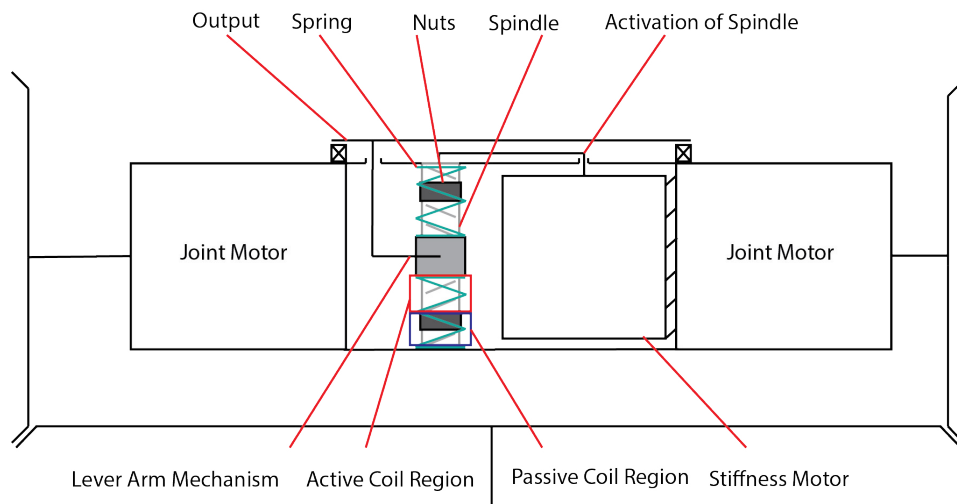


Figure 2.5: Adaptation of the 'Jack Spring' towards use in the Differential Drive.

Fig. 2.5 depicts the 'Jack Spring' integrated into the DD. In this particular design two springs are connected to the output and the active and passive coil regions are

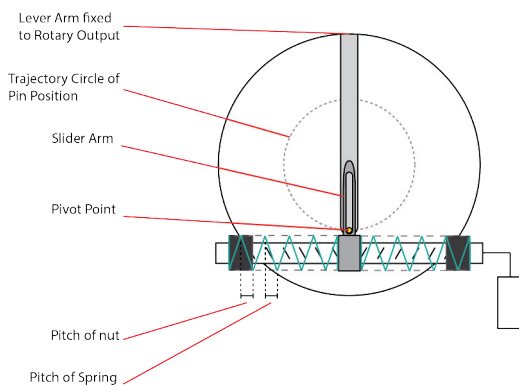


Figure 2.6: Eq. Position of Jack Spring in DD

divided by two nuts, which run on a spindle with opposite threading. Subsequently the spindle is actuated by the stiffness motor connected rigidly to both joint motors. The linear motion of the output of the springs has to be converted into a rotation by means of a lever arm, also shown more clearly in fig.

2.6. The main issue with this type of variable stiffness mechanism is the adjustment of the stiffness when the springs are not in equilibrium position. This is made clear by fig. 2.7. The relative pitch diameter of nut and spring change under load conditions. The effect of this could be undesired behavior of the output deflection. Additionally the springs are attached to a slider moving across the spindle and will cause friction. The big advantage however still is that the motor does not pretension the springs, thus the design is more energy efficient compared to the 'Spring

Preload' mechanisms.

The chosen alternative to the 'Jack Spring' implementation is illustrated in fig. 2.8 and is founded on the 'VS-Joint' and 'FSJ' mechanisms. The rigidly connected cam profiles are located in the middle of the two joint motors. This design is comparable to an inverse of the 'FSJ' principle. However instead of having a hollow spring in the middle of the design the cam profiles are connected via shafts to the joint motors. The thought behind this is that conventional springs can be used instead of one custom made spring with a high spring constant and it is presumed that less

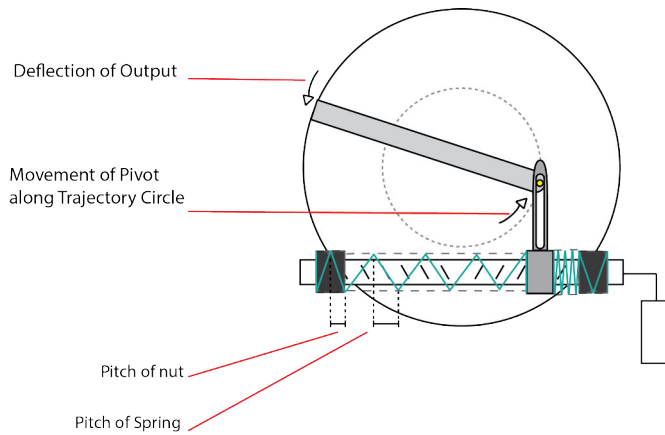


Figure 2.7: Deflection of Jack Spring in DD.

space is consumed by employing a rigid connection through the middle of the design. Additionally the springs are connected to rollers on one side, which is similar to the 'VS-Joint' and to rotating cups on the other side. This is contrary to the 'FSJ' where the spring is attached to both cam profiles. The function of the rotating cups is to adjust the relative position of the rollers on the cam profiles to change the stiffness. Hence the stiffness motor rotates the cups against each other. The problems of this design mainly focus

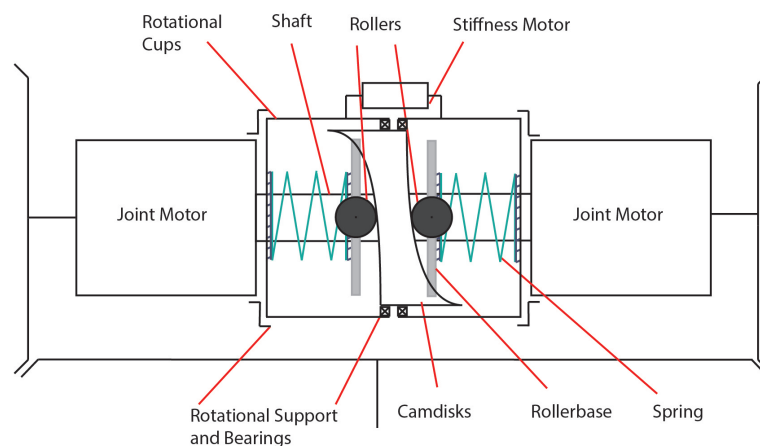


Figure 2.8: Adaptation of the Pretension Mechanism of 'DLR' towards use in the Differential Drive.

on the stiffness motor that has to withstand the maximal applicable torque of $100Nm$. To reduce a loss of energy a break should be implemented, so the motor does not have to supply a constant torque against an output deflection. Another criteria for the choice is the compactness of the design, which highly depends on the spring

element since it has to cope with the high torque. The 'Jack Spring' actuator uses two springs as well as the alternative design. The roller-base and orientation of the springs in the shaft direction leaves more space to make use of bigger or multiple springs in the preload design.

The implementation of the 'Jack Spring' mechanism has more obstacles to overcome, referring to the friction of the slider on the threaded shaft and the problems due to the difference in pitch diameter during deflection. Besides the pretension mechanism leaves more room for adaptation of multiple springs. So even if a break has to be implemented the choice was made towards the design shown in fig. 2.8 .

Chapter 3

Modelling

3.1 Analysis of Variable Stiffness Mechanism

The chosen mechanism has to fulfill the requirements of $100Nm$ Output Torque, which is targeted by analyzing the variable Stiffness Mechanism in depth. Initially the output torque for different spring arrangements was calculated as in [15] and is subsequently checked by a more force approach.

3.1.1 Torque-Deflection Characteristics

In [15], s is the state of the spring and the elastic energy is given by $H(s)_s = \frac{1}{2}ks^2$, where k is the elastic constant of the spring". Therefore the state of the spring can be expressed as a function of the displacement of the spring due to the cam disk profile as shown in Figure 3.1, where $\Delta x = s(\varphi)$. The cam profile has an exponential shape and s depends on the deflection of the rollers on the cam disk φ , the stiffness preset ϕ , the maximum allowable displacement s_{max} of the spring at φ_{max} and the displacement S_0 at $\varphi = 0^\circ$. The state of spring can be described as follows:

$$s(\varphi) = S_0 e^{b\varphi} \quad (3.1)$$

,where S_0 is chosen, depending on how sensitive the VSM should be and should not exceed φ_{max} of course. The parameter b in eq. 3.1 can be determined by inserting s_{max} and φ_{max} into the equa-

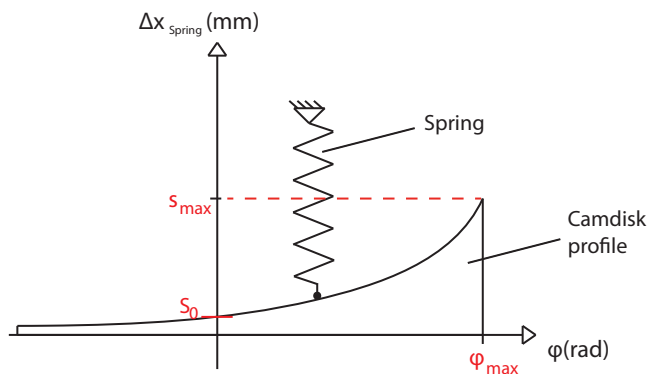


Figure 3.1: State of Spring as Function of Deflection φ on Cam disk.

tion, i.e. :

$$b = \frac{\ln\left(\frac{s_{max}}{S_0}\right)}{\Phi_{max}}, \text{ where } s_{max} = l_f - l_s \quad (3.2)$$

The maximum displacement can be calculated by subtracting the solid length l_s from the free length l_f of the chosen spring.

Next the Output torque has to be defined by making use of the state of the spring. From [15] it can be obtained that the Force F at the Output Port can be described as $F = -B^T(q, r) \frac{\partial H_e}{\partial s}(s)$. Noting that $H_e(s)$ is the elastic energy of the compliant element and $B(q, r)$ is the sub-matrix defining "the relation between the rate of change of the output position r and the rate of change of the state s of the elastic elements" [15]. The latter can be described as $B(q, r) := \frac{\partial \lambda}{\partial r}(q, r)$. According to Visser $\lambda : (q, r) \mapsto s$, so that $B(q, r) := \frac{\partial s}{\partial r}$. This can be inserted into the Force equation and finally eq. 3.3 can be obtained.

$$F = -\frac{\partial s}{\partial r} \frac{\partial H_e}{\partial s}(s) \quad (3.3)$$

The state of the spring s defined earlier however is expressed by the Output deflection φ in radians and not in output position r . Therefore $\varphi = \frac{r}{r_c}$, with r_c being the radius of the cam disk, has to be substituted into the displacement equation, such that $s(r) = S_0 e^{b \frac{r}{r_c}}$. Additionally eq. 3.3 should be defined as a output torque of a spring on a cam disk by multiplying with the radius of the cam disk r_c . Accordingly eq. 3.3 is adapted and $H(s)_s$ and $s(r)$ are inserted respectively, resulting in eq. 3.5 below.

$$r_c F = \tau_{cam} = -r_c \frac{\partial s}{\partial r} \frac{\partial H_e}{\partial s}(s) = -r_c \frac{\partial s}{\partial r} k s \quad (3.4)$$

$$= -k r_c \frac{b}{r_c} S_0^2 e^{2b \frac{r}{r_c}} = -k b S_0^2 e^{2b \frac{r}{r_c}} \quad (3.5)$$

Resubstituting of $\varphi = \frac{r}{r_c}$ results in:

$$\tau_{cam}(\varphi) = -k b S_0^2 e^{2b \varphi} \quad (3.6)$$

Last but not least the output torque is also affected by the stiffness preset which is set by the stiffness motor and changes the apparent output stiffness. In order to change the Stiffness the motor has to move the position of the springs on the cam disks relative to each other as shown in figure 2.8 by ϕ . The resulting Output torque is shown below:

$$\tau_{cam}(\varphi, \phi) = -k b S_0^2 e^{2b(\varphi + \phi)} \quad (3.7)$$

3.1.2 Torque-Deflection Plots

To realize the target of $100Nm$ output torque different spring setups and deflection ranges have been investigated. When plotting the torque-deflection it is important to sum up the output torques of the opposing cam-mechanisms to get the total output-torque τ_{ext} as in eq. 3.10.

$$\tau_{cam(up)}(\varphi, \phi) = kbS_0^2 e^{2b(\varphi+\phi)} \quad (3.8)$$

$$\tau_{cam(down)}(\varphi, \phi) = -kbS_0^2 e^{2b(-\varphi+\phi)} \quad (3.9)$$

$$\tau_{ext} = \tau_{camup} + \tau_{camdown} \quad (3.10)$$

Consequently the springs and their alignment in the mechanism have to be chosen. For this setup Die-Springs were used, because they can handle heavy duty (see [23]) and thus have a higher spring constant k , compared to common compression springs, with the same dimensions. The springs setups used for the first torque-deflection plot are a single Die-Spring and four Die-Springs in parallel connected to the rollers on the upper and lower cam profiles. The implementation of four springs is motivated by the possible adaptation of multiple springs as discussed in section 2.2 to achieve a higher output torque. To stay within the specified limits of $100mm$ length, the springs should not exceed a free length of $l_f \leq 40mm$. Additionally the single Spring should have a diameter that is large enough to leave enough space for a shaft passing through. The four springs on contrary are positioned around the shaft. Thus it is of importance that they fit within the specifications of $130mm$ in diameter of the mechanism. To accomplish the latter, the cam disks have been given a radius of $r_c = 40mm$ and the diameter of the parallel arranged springs has to fit in between the cam profile and the shaft as shown in 3.2. A rough estimate

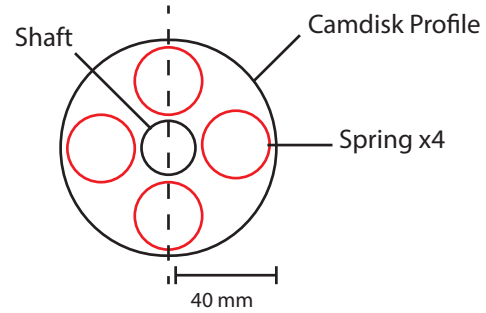


Figure 3.2: Different Spring Setups

provides that the diameter of the parallel springs has to be smaller than $20mm$. Next the spring components are chosen depending on the requirement to fit into the VSM. Eventually the spring [24] was chosen as the single spring setup with $k = 144.45N/mm$ and $l_f = 38.1mm$. The spring for the parallel setup is [25] with a spring constant of $k = 47.62N/mm$, the same free length as for the single setup and a outer diameter of $D_0 = 14.808$. Since there are four springs in parallel the resulting spring constant is $k = 190.48 N/mm$. The deflection range for this first attempt was set to $\varphi = [-15 \ 15^\circ]$ and will be evaluated further in a second plot. S_0 is set to $3.1mm$ at $\varphi = 0^\circ$. The torque on the cam profiles was calculated as described in

subsection 3.1.1 for each spring setup and eventually the total output-torque was calculated by making use of eq. 3.10. This can be seen in fig. 3.3. To review the entire calculation, the MATLAB file can be checked in APPENDIX A (A.1 - A.3).

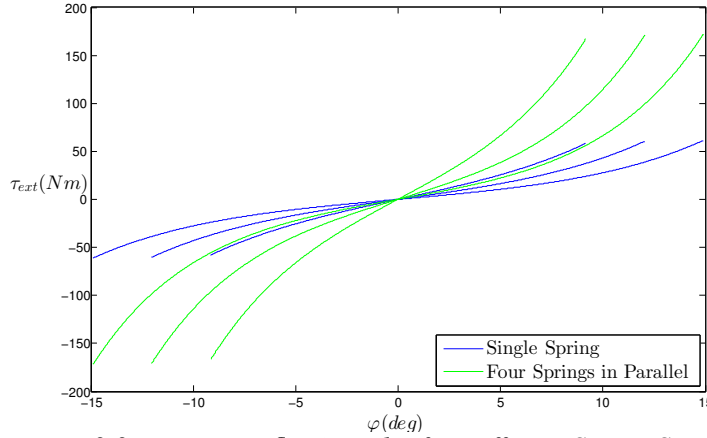


Figure 3.3: Torque-Deflection Plot for Different Spring Setups

In fig.3.3 each of the spring-setups have three subplots. This is because every plot was made with three different stiffness presets of $\phi = 0, 0.05$ and 0.1 [rad]. Analyzing this first Torque-Deflection plot, it can be stated that due to a lower stiffness preset the total Output torque has a smaller total deflection, which is what would be expected. Besides, the total Output-Torque for the setup using multiple springs on each side is higher than the Output-Torque for the single spring setup. This has two main reasons. First of all the spring constant is higher and secondly each spring has

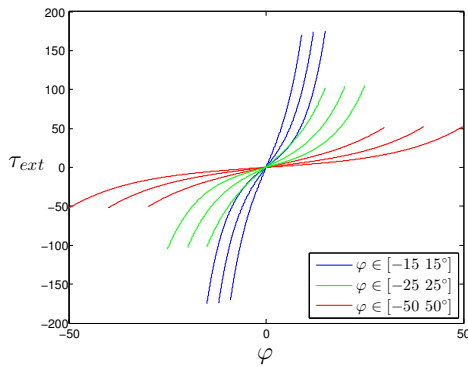


Figure 3.4: Deflection Range

a greater allowable displacement, because each individual spring is more compliant than the single-spring setup. All in all, this plot encourages the choice for multiple spring-setup, also because if using a single spring with the same free length l_f , the diameter of the rod will become rather small, when trying to achieve the same Output-Torque amplitude.

In the following part, the analysis will focus on the Deflection-Range of the cam-profile to realize the required $100Nm$. The Deflection-Range has an impact on the torque amplitude due to the fact that it also scales the b parameter of the state of the spring s (ref. eq.3.2). Such that each state of spring for a chosen deflection had to be recalculated before plotting, including the spring characteristics for the parallel spring-setup. The chosen ranges are depicted in fig.3.4 and also here different Stiffness-Presets by changing ϕ to 20% and 40% of each particular deflection range is included. Taking a closer look at the

plots in APPENDIX A fig.A.4 reveals that at $\varphi = 25^\circ$ the Output torque is $105.3Nm$. Concluding it is to mention, that the deflection range of $\varphi = [-25\ 25^\circ]$ is closest to the target Output-Torque. Thus this range is applied to the design of the mechanism together with four springs in parallel on each side.

3.1.3 Force Approach

The former approach to calculate the Output torque depending on deflection φ and stiffness preset ϕ is based on a method given by [15]. To confirm this method a more fundamental approach has been investigated, based on a force model of the mechanism. When the spring is compressed, due to movement of the rollers on the cam-profile, it creates a force F_s acting on the cam profile, as illustrated in fig.???. The resulting Forces acting on the exponential profile are F_N acting normal to the profile and F_{10} , which is the output force. For the sake of retrieving the total output Force F_{tot} , the output force F_{10} has to be evaluated in every point x_0 on the 2D-profile and summed up with the output force on the opposing profile F_{20} . Lastly the total output force will be converted into torque τ_{ext} by multiplying with $r_c = 40mm$. Primarily the displacement of the spring has to be rewritten to be dependent on x and not on φ , by inserting $\varphi = x/r_c$. So equation 3.1 transforms to

$$s(x) = S_0 e^{\frac{b}{r_c}x} = 3.1 e^{\frac{3.2846}{40}x} \quad (3.11)$$

Based on the Force of the spring $F_s = ks(x)$ and the angle α all other forces in the model can be expressed as follows:

$$F_N = \frac{1}{\cos(\alpha)} F_s \quad (3.12)$$

$$F_{10} = \sin(\alpha) F_N \quad (3.13)$$

At this moment all parameters are defined except angle α , which can be calculated by making use of the slope m of s . The slope m is equal to the derivative of s in x_0 (3.14).

$$m = \tan(\alpha) = \frac{\partial s(x_0)}{\partial x} \quad (3.14)$$

$$\alpha = \tan^{-1}\left(\frac{\partial s(x_0)}{\partial x}\right) \quad (3.15)$$

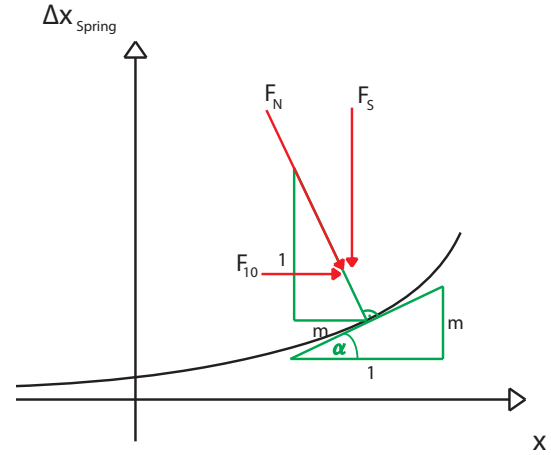


Figure 3.5: Force representation of the VSM mechanism.

The plots and MATLAB-file can be reviewed in APPENDIX A (fig.A.5 and fig.A.6-A.8). Fig.A.5 illustrates that the force approach is indeed identical to the former method. However this can also be proofed in a more simple manner. Inserting equation 3.13 into equation 3.12 and eventually substituting $\tan(\alpha)$, leads to

$$\frac{F_{10}}{\sin\alpha} = \frac{1}{\cos(\alpha)} F_s \quad (3.16)$$

$$F_{10} = \frac{\sin(\alpha)}{\cos(\alpha)} F_s = \tan(\alpha) F_s = m F_s = \frac{\partial s(x_0)}{\partial x} F_s \quad (3.17)$$

The result is identical to eq.3.3.

3.1.4 Apparent Output Stiffness

A plot was made of the output-stiffness against the output-torque, calculated in the previous sections. As in [15], the apparent output stiffness K can be described as the ratio of the infinitesimal change of the actuator output force ∂F , as a result of an infinitesimal displacement of the actuator output position ∂r . In the case of the cam mechanism this can be reformulated to $K = \frac{\partial \tau_{cam}}{\partial \phi}$. The result of this rather simple calculation can be viewed in fig.3.6.

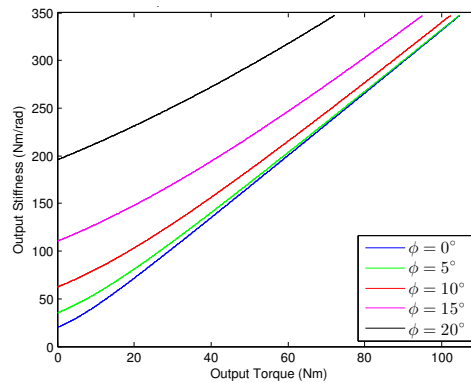


Figure 3.6: Output Stiffness for different stiffness presets, starting with $\phi = 0^\circ$, so very compliant and ending with a stiff preset of $\phi = 20^\circ$

The figure confirms that the stiffness preset ϕ is included correctly in the output-torque equation, since for a compliant setting of $\phi = 0^\circ$ the mechanism is at its most compliant with about $K = 20Nm/rad$ at low torque-output. Vice versa the highest Stiffness at low torque-output of $K = 195Nm/rad$ is achieved for $\phi = 20^\circ$. The highest Stiffness can be achieved however with every stiffness preset of ϕ , because the relative position of the springs on the profile can be changed such that they can not achieve minimum stiffness anymore but can still roll up the cam profile.

3.2 Motoranalysis

This section emphasises on Power-, Volume- and Dynamic Analysis to gain insight into the requirements of the motor. The specifications obtained by the different analysis serve as a feasibility study for the motor including gearbox to fit into the design and comply with the given requirements of 100 Nm output torque.

3.2.1 PowerAnalysis

To identify the parameters necessary to make a Power-analysis other variable stiffness actuators, their Nominal Stiffness Variation Times and Nominal Speed characteristics have been investigated. The vsaUT-II provides a Nominal Stiffness Variation Time of 0.6[s] with a Nominal Speed of π [rad/s], while the FSJ provides values of 0.33[s] and 8.51[rad/s] respectively.

The Power will be determined by using the average torque τ_{avg} [Nm] and angular velocity (Speed) ω_{avg} [rad/s], as described in:

$$P_{avg} = \omega_{avg} * \tau_{avg} \quad (3.18)$$

The average torque (τ_{avg}) can be obtained by taking the average of the maximum and minimum torque required to get a completely stiff and compliant setting of the VSM, i.e.:

$$\tau_{avg} = \frac{\tau_{max} + \tau_{min}}{2} \quad (3.19)$$

In order to change the Stiffness, both of the opposing spring mechanisms have to be either compressed or expanded at the same time. This means that in order to get the maximum torque at an angle of $\sigma_{max} = 25^\circ$ for both cam disks, the maximum torque obtained through $\tau_{camdisk}(\sigma_{max})$ has to be multiplied by 2. The minimum torque is computed the in the same manner except that $\sigma_{min} = 0.1^\circ$. So by calculating $\tau_{camdisk}$ with respect to σ we get:

$$\tau_{camdisk} = \frac{ds}{d\sigma} ks \approx 5999.5e^{6.6\sigma} \quad (3.20)$$

Inserting σ_{max} , σ_{min} and multiplying by 2 results in:

$$\tau_{max} \approx 209.135[Nm], \text{ at } \sigma_{max} \quad (3.21)$$

$$\tau_{min} \approx 12.137[Nm], \text{ at } \sigma_{min} \quad (3.22)$$

And by making use of Equation (3.19) we get $\tau_{avg} \approx 110.636[Nm]$.

The average angular velocity can be calculated by the following equation:

$$\omega_{avg} = \frac{2\sigma_{avg}}{t_{nom}} \quad (3.23)$$

where t_{nom} is the Nominal Stiffness Variation Time chosen for this VSA and σ_{avg} is the nominal angle, which can be calculated by using τ_{avg} as follows:

$$\frac{\tau_{avg}}{2} \approx 5999.5e^{6.6\sigma_{avg}} \quad (3.24)$$

$$\sigma_{avg} \approx \frac{\ln\left(\frac{\tau_{avgnom}}{11999.1}\right)}{6.6} \quad (3.25)$$

and thus the nominal angle of $\sigma_{avg} \approx 0.3391[rad]$.

The Nominal Stiffness Variation Time was chosen to be $t_{nom} = 1[s]$, despite the Stiffness Variation Times of investigated VSAs, compensating for the high nominal torque in eq. (3.19). The necessity of this measure evolves from the fact that the power-consumption has to be kept low to allow a usage of small motors, which still fit into the design. Based on the calculated values and equation 3.23, the average angular velocity is $\omega_{avg} \approx 0.678[rad/s]$. Equation 3.18 then gives $P_{avg} \approx 75.039[W]$.

3.2.2 Transmission Analysis

The ‘Robotic Optimized Servodrive’ series (TQ Robodrive) was chosen to be used, since the dimensions have to be kept compact. The TQ Robodrive enables the latter by offering the possibility to design customized housings for the chosen motor. Different types of the "Robodrive" permit different input torques τ_{in} , which will be obtained from the figures in the Appendix by calculating the current amplitude I_{in} . The current amplitude can be calculated by taking the rated voltage of 24V and 48V and the previously determined Power P_{avg} . Taking $P_{avg} = I_{in}V_{in}$ results in $I_{in} = 3.126 A$ and $I_{in} = 1.563 A$ for $V_{in} = 24, 48V$ respectively. Due to these values for I_{in} values for the input torques τ_{in} can be obtained from the figures in the APPENDIX B and are depicted in Tab. 3.1. The values for the ‘ILM 25x08’ and ‘ILM 38x06’ by ‘TQ-Group’ are about the same, thus there is only one row in Tab. 3.1 for both.

To continue with the Volume Analysis, it is necessary to know the size of the gear, that has to be combined with the motor in order to get the desired average torque of $\tau_{avg} \approx 110.636[Nm]$. The size of the gear can be estimated by calculation of the gear ratio r , which depends on the input torque τ_{in} , the average torque τ_{avg} and the

efficiency of the gearbox η , as shown in eq. (3.26).

$$r = \frac{\tau_{nom}}{\eta\tau_{in}} \quad (3.26)$$

The gear mechanism has to be non-back-drivable, such that the stiffness motor does not have to supply constant torque and subsequently the energy efficiency of the VSA is increased. To ensure that the gear ratio will not increase significantly due to inefficiency caused by the use of for example worm gearboxes, hypoid gears can be used as non-back-drivable elements. The efficiency η of worm gears can be as low as $\eta = 0.3 \%$, while the efficiency of hypoid gears is about $0.85 \leq \eta \leq 0.96 \%$ as shown in [16]. To get a worst case estimation, the lowest efficiency of $\eta = 0.85$ is taken and results are depicted in Tab. 3.1 together with the input torques τ_{in} .

	ILM 25x08/ILM 38x06		ILM 38x12		ILM50x08	
	$\tau_{in} [Nm]$	r	$\tau_{in} [Nm]$	r	$\tau_{in} [Nm]$	r
24 V	0.051	2552.16	0.11	1183.27	0.25	520.64
48 V	0.024	5423.33	0.055	2366.54	0.125	1041.29

Table 3.1: Values for input torque τ_{in} and gear ratio r with $\eta = 0.85$

Tab. 3.1 already points out that the gear ratios are at a level where the implementation of a single stage gear becomes obsolete. Therefore high efficient Harmonic Drives could be implemented together with a hypoid gear. If using a worm-gearbox the mechanism would probably consist of two gear stages and the worm gearbox to achieve the necessary gear ratio. Values for the gear ratio when implementing a worm gear are shown in table 3.2.

	ILM 25x08/ILM 38x06		ILM 38x12		ILM50x08	
	$\tau_{in} [Nm]$	r	$\tau_{in} [Nm]$	r	$\tau_{in} [Nm]$	r
24 V	0.051	7231.11	0.11	3352.61	0.25	1475.15
48 V	0.024	15366.11	0.055	6705.21	0.125	2950.29

Table 3.2: Values for input torque τ_{in} and gear ratio r with $\eta = 0.3$

Tab. 3.1 and Tab. 3.2 show that an implementation of the smallest motor is basically not possible because the gear ratio is at a level where we would have to use a really bulky gear mechanism with a lot of stages contradicting the goal of compactness. The "14-CSD-2A" thin "Harmonic Drive" (ref. [27]) could be used, which can achieve a gear ratio of $r = 100$ and is the smallest and thinnest of the Harmonic CSD-Series. Next the left over gear ratios are depicted in Tab. 3.3 and Tab. 3.4 dividing the gear ratio of the HD and neglecting the smallest motors.

	<i>ILM38x12</i>	<i>ILM50x08</i>
24 V	11.83	5.21
48 V	23.67	10.41

Table 3.3: Values for gear ratio r with $\eta = 0.85$ divided by r_{HD}

	<i>ILM38x12</i>	<i>ILM50x08</i>
24 V	33.5261	14.75
48 V	67.05	29.5

Table 3.4: Values for gear ratio r with $\eta = 0.3$ divided by r_{HD}

The left over gear ratios in tab. 3.3 can be achieved with the harmonic drive and a hypoid gear, whereas the gear ratios from tab. 3.4 probably need a second gear stage or an extra harmonic drive before the worm gear stage, but this still depends on the efficiency of the chosen worm-gear.

An alternative to a bulky gear mechanism due to the use of a non-back-drivable gear element was developed by replacing the non-back-drivable element by clutches. If the gear mechanism is smaller a bigger motor with higher input torque can be used and the implementation of a single gear stage becomes arguable. On top of that the clutches do not have a drawback caused by lower efficiency which means that in a setup without non-back-drivable gear element the efficiency can be set to $\eta \approx 1$. The "ILM70x10" and "ILM-85x13" are the thin versions of the big "Robodrive" have nominal input torques of $\tau_{nom_{in}} = 0.74[Nm]$ and $1.43[Nm]$ at a nominal power consumption of $P_{nom} = 270[W]$ and $450[W]$ respectively according to [26]. Important to mention here is that the input torque at lower power consumption, like $75[W]$ is not significantly higher than in the previous calculations. However these motors have a broader performance range and therefore enable higher input torques, at cost of larger power consumption. Using the former calculation of gear ratio with efficiency $\eta = 1$ and the nominal input torques of the bigger motors, results in table 3.5.

	<i>ILM70x10</i>	<i>ILM85x13</i>
r	149.51	77.37

Table 3.5: Gear ratio r based on $\tau_{nom_{in}}$ and τ_{avg} for additional motor models

These gear ratios can definitely be handled by a single gear stage like the "25-CSD-2A Harmonic Drive" (ref. [27]) with a gear ratio of $r = 160$. Another advantage of the smaller gear ratios in tab.3.5 and higher power consumption is that the angular input velocity ω_{in} will be greater and the nominal Speed and Stiffness variation time of the VS-mechanism will benefit compared to the smaller motors.

3.2.3 Volume Analysis

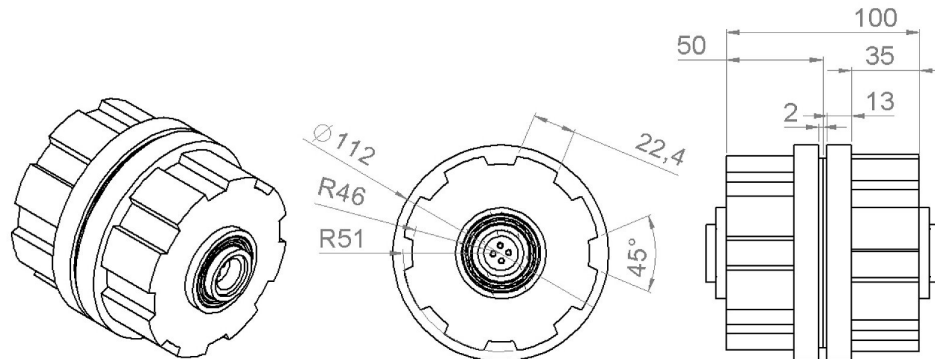


Figure 3.7: 2D-View of the Assembly without Motor, all dimensions in mm.

Fig.3.7 shows a 2D-Representation of the VS-mechanism in this report. The VS-Mechanism depicted already gives a preview to the Design chapter and will help with the volume analysis. The goal of this section is to find a placement of the motor and gear such that the entire module does not exceed the dimensional limits of 130mm in diameter and 150mm in length. The Volume Analysis starts with a possible arrangements of the motor with respect to the variable stiffness mechanism, shown in tab. 3.6.

	<i>Radial</i>	<i>Axial</i>
⊥		

Table 3.6: Possible Arrangements of Motor. Upper horizontal column displays the placement of the motor in radial or axial position to the VS-mechanism. left Vertical row displays the shaft alignment of the VS-Mechanism as either parallel or perpendicular.

In the table above the VS-mechanism is represented as the rightmost 2D-representation from figure 3.7. The shafts on the right and left in each figure in the table serve as the connections to the differential drive. The motor is illustrated as a red rectangle with possible shaft arrangements shown as black lines in the middle of the motor. The four different arrangements are distinguished by perpendicular or parallel shaft

alignment of the motor shaft to the VS-shaft and in axial or radial placement of the motor to the VS-mechanism. From this simple diagram the different possibilities in gear combinations can be derived and evaluated.



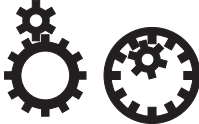

	Possible Transmission	Transmission Ratio	Efficiency	Compactness	Costs
⊥	 <i>Custom Bevel Gears</i>	+/-	+	+	-
	 <i>Worm gearbox</i>	+	+/-	-	++
	 <i>Spur gears</i>	-	+	+	+/-
	 <i>Pulley System</i>	-	+	-	+

Table 3.7: Possible gear and non-back-drivable element addition to previous motor arrangements.

For the perpendicular shaft alignment of stiffness mechanism and motor, custom bevel gears or a worm gearbox can be used, whereas for parallel alignment spur gears or a pulley system can be chosen referring to tab. 3.7. As shown in previous chapter when relying on a small motor at least one other gear stage in terms of a harmonic drive has to be implemented together with each of the gears in the table above. Whilst the perpendicular arrangements already enable non-back-drivability, the gears for the parallel shaft alignments have to be decoupled by using clutch mechanisms.

Now the advantages and disadvantages of each setup will be explained and discussed. The Bevel gear has to be custom made since it should also be non-back-drivable. Therefore the costs will be high but the mechanism can be held quiet compact. The possible transmission ratio could be within the limits but has to be

evaluated further by the manufacturer. Especially hypoid gears are known for their high transmission ratios. As explained earlier in this section the efficiency of bevel gears is rather promising compared to worm gearboxes because the friction component -which makes worm gears non-back drivable- is higher at lower speeds. Due to the small size of the worm the allowable transmission ratio offers a promising range of upper limit values. The worm gear is available as complete gearbox modules; lowering the costs but affecting the compactness negatively. The gears depicted in 3.7 for a parallel arrangement of motor and mechanism shaft have similar characteristics concerning the transmission ratio and efficiency on one hand. Comparing the compactness however the pulley system has to be placed further apart and thus occupies more space in the mechanism. The Spur gear would probably have to be custom made to fit into the requirements of the mechanism affecting the costs. It is however less expensive than the custom made bevel gear.

3.2.4 Choice of Motor and Gear Combination

Concluding the motor analysis, a comparison is made between the transmission for different motor types as shown in subsection 3.2.2 and available gear combinations evaluated in subsection 3.2.3. The smaller motor models (tab. 3.1) are in need of a higher transmission than the bigger robodrive models. Thus a perpendicular shaft alignment should be chosen according to tab. 3.7 since the bevel gear and worm gear offer greater transmission ratios. Furthermore the bevel gear would have to be made by a specialist in order to be non-back-drivable or a clutch has to be added. Thus the worm-gearbox should be used together with a harmonic drive for a small motor.

If using a bigger motor (tab. 3.5) a parallel shaft alignment can be chosen since the needed transmission ratios are smaller. Additionally the inner diameter of the bigger motor models is sufficiently large enough to make the mechanism shaft pass through and use a hollow spur gear, which is more compact than a pulley system or harmonic drive. If using a harmonic drive the gear stages can be reduced to a single gear stage and a clutch mechanism ensuring self locking of the mechanism.

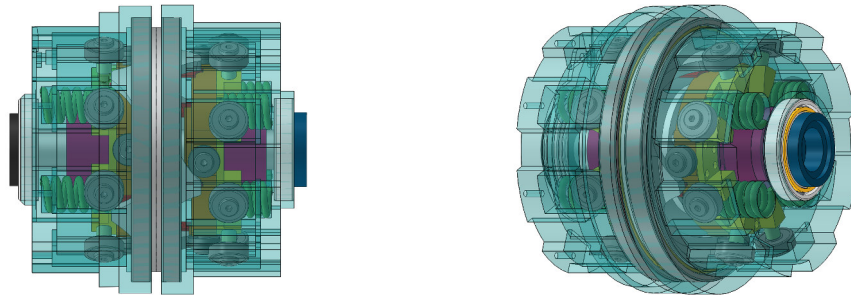
Both of the just mentioned motor- gear combinations are using off-shelf components, which makes them cheaper than the other arrangements. The combination with the bigger motor uses a clutch mechanism which has to be researched in depth. The multiple stage gear for perpendicular shaft alignment is harder to realize, offers however a built-in self locking mechanism. In the end the parallel shaft alignment was chosen with a 'ILM70x10' and a '25-CSD-2A Harmonic Drive', since it is more compact.

Chapter 4

Design

The design chapter consists of two parts about the realization of the variable stiffness mechanism and of the Stiffness Actuation relying on the decision made in section 3.2 respectively. The Drawings were done in 'SOLIDWORKS2012'. Special attention in the design of the VSA is paid to the dimensional requirements given as 100[mm] length and 130[mm] in diameter.

4.1 Variable Stiffness Mechanism



(a) Front View of Preload Mechanism with transparent Rotational Cups

(b) Side View of Preload Mechanism

Figure 4.1: Overview of Design of Variable Stiffness Mechanism

According to section 3.1 the compliant mechanism has to include four springs on each side of the cam-disks shown in fig. 3.2 and the exponential cam profile specified in equation 3.1 with the chosen spring and a deflection range of $\varphi = [-25^\circ \ 25^\circ]$. Thus the state of spring on the profile should be $s_{cam}(\varphi) \approx 3.1e^{3.2846\varphi}$ with φ in [rad]. The final mechanism is shown in fig. 4.1 and has dimensions of

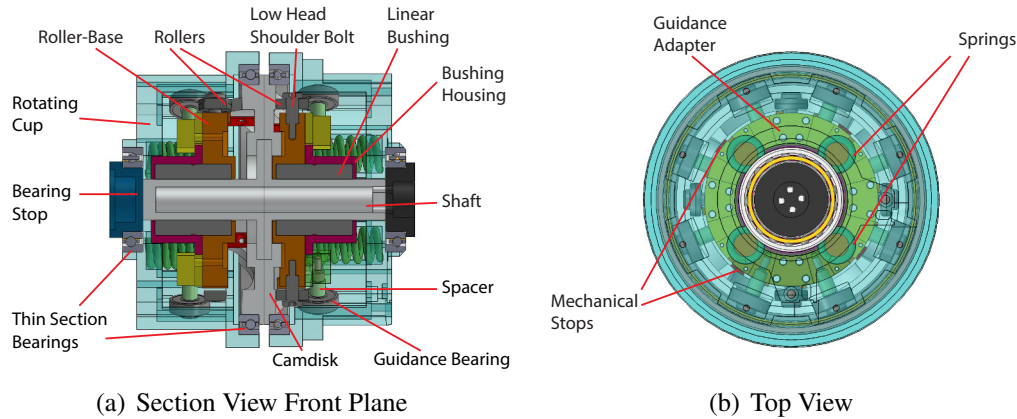
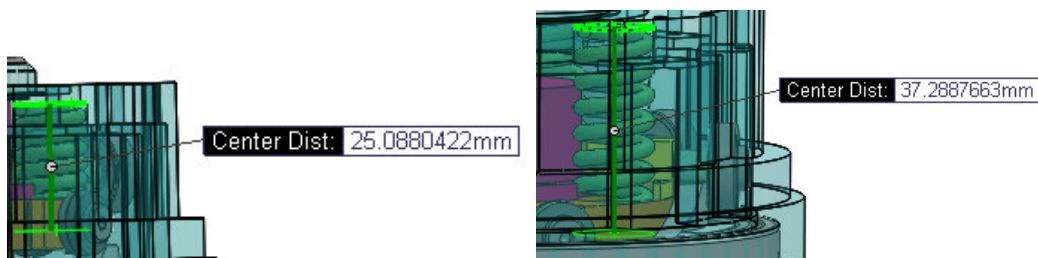


Figure 4.2: More Detailed View of Design

100[mm] in length and 115.138[mm] as its maximum diameter.

All different components and their labels can be viewed in Section View 4.2a) and Top View 4.2 b). The main shaft has to be connected via Bearing Stops to the joint motors (ref fig. 2.8) on each side and is attached to the opposing cam disks in the middle. The specified cam profile has an offset of 6.5 [mm], because radius of the cam rollers, which are ball bearings ([28]) in this case has to be taken into account. The rollers are mounted by 'Low Head Shoulder Bolts' [29] to the roller-base. The roller-base and the rotating cup define the endpoints of the spring. At this point it has to be taken heed of that the length of the spring at minimum deflection can not exceed $l_f - s_{cam}(\varphi_{min}) \approx 38.1 - 3.1e^{3.2846(\frac{-25\pi}{180})} \approx 37.3605$ [mm] and $38.1 - 12.995 = 25.105$ [mm] for maximum deflection, this is verified when taking a look at illustration 4.3. The real values differ by 0.0717337 [mm] and 0.0169578 [mm] for the roller in minimum and maximum position on the profile. This also proves that the offset given to the calculated shape of the profile is correct. The rotational cups have to rotate together with the roller-base considering that a



(a) Spring length for maximal deflection of 25° (b) Spring length for minimal deflection of -25°

Figure 4.3: Exact Measurements of the Spring Space for Extreme Cases.

linear deformation of the spring in shaft direction is an objective for proper function of the mechanism. Therefore linear guidances in form of bearings (also [28]) that can roll in axial direction along small cavities in the rotational cups (ref. fig. 4.1 b)

have been implemented. The so called guidance bearing is as well fixed with a shoulder bolt, via guidance adapters (yellow parts) to the roller-base. Additionally the roller-base should be centered around the shaft, which is achieved by a linear bushing [30] on each side. The linear bushing is attached through a housing to the roller-base. The rotational cups have to be supported on each side by Thin section bearings with bore diameter of $25[mm]$ [31] and $90[mm]$ [32] The small thin section bearings are supported on the other side by bearing stops, which can later on be connected to the differential drive. In this way the Springs are pressed together by the roller-base and the rotational cup.

4.2 Motor and Gear Module

At this stage it got obvious that it is impossible to fulfill the dimension requirements, because the previously designed stiffness mechanism has already reached dimensional limitations that make the design of the motor within the given requirements unfeasible. It could be argued that there is still space in the radial direction, but even with a small motor the gear system will be too bulky, which is proved in subsection 3.2.2. On these grounds the requirements were adapted to $150[mm]$ in length and still $130[mm]$ in diameter. The entire variable stiffness actuator is represented in fig. 4.4. Its uttermost dimensions are $153.6[mm]$ in length and $135[mm]$ in diameter.

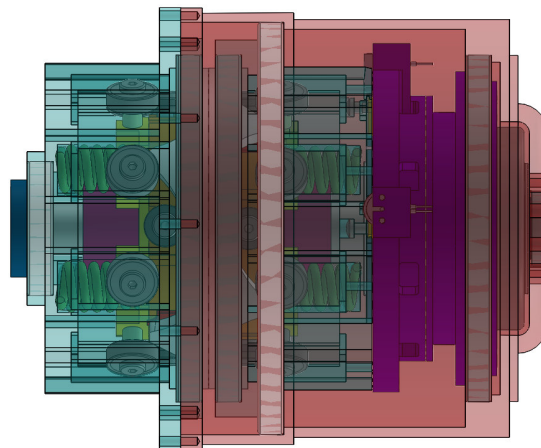


Figure 4.4: Variable Stiffness Joint including Motor, Gear and Clutch System.

All different Components and connections can be seen more clearly in the Section View in fig. 4.5 a). The objective of the motor and gear system is to rotate the support cups relative to each other to manipulate the stiffness. Hence, the Stator of the

'TQ-Robodrive ILM70x10' is fixed to the right rotating cup via the Stator Housing whilst the Rotor has to be connected through the '25-CSD-2A Harmonic Drive' to the left rotating cup. The stator housing is also attached to the circular spline on the right side to hold the 'Harmonic Drive' in position. The Rotor axle is attached to the input, also called wave generator of the HD and is rotationally supported by carrier bearings with bore diameter 20[mm] [33] and 17[mm] [34]. In order to understand the drawing it should be noticed, that the shaft extension mounted to the main shaft of the mechanism still has to be attached to the differential drive, which is why the rotor housing and the HD are hollow. Last but not least the Output of the harmonic drive - the flex spline - is linked to the left rotating cup via the gear connection cup. The gear connection cup is stored by two thin section bearings with bore diameter 90[mm] [32] and 110[mm] [35].

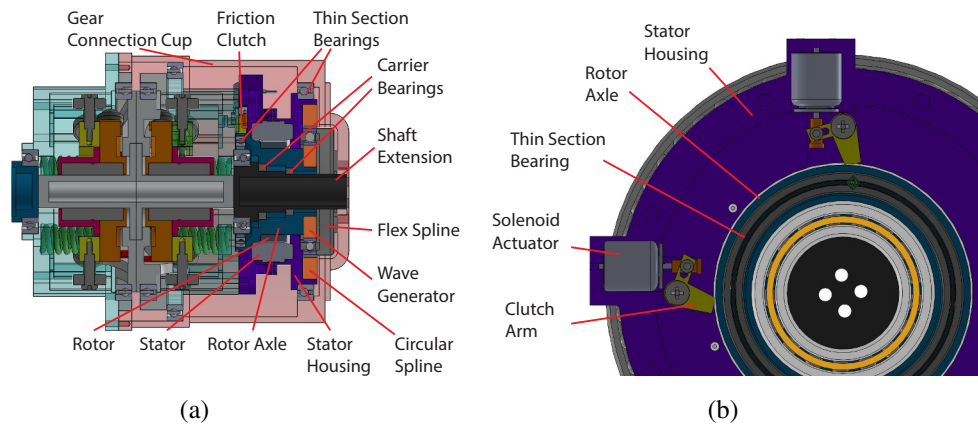


Figure 4.5: Labeled Section View of Variable Stiffness Joint in a) and the friction clutch integrated into the Variable Stiffness Joint in b)

Another thin section bearing([36]) supports the rotor axle on the same position, where the friction clutch is located, as can be seen more detailed in fig. 4.5 b). The friction clutch is designed with a logarithmic profile and a contact angle of 8° according to [17] and can withstand torques up to 2[Nm] which is smaller than the nominal torque of the 'Robodrive' (0.74[Nm]). The Push and Pull Solenoid [37] is mounted to the Stator housing and actuates the clutch arm to cause friction on the rotor axle. This way the motor can be decoupled from the mechanism.

4.3 Datasheet

Due to the broad range of variable stiffness actuators and their different fields of application, a VSA datasheet has been developed in [18], which can serve as a set-point for the comparison of the developed mechanism for postprocessing. The Design and Modelling chapters provide the input for said datasheet and the result can be seen below in tab. 4.1.

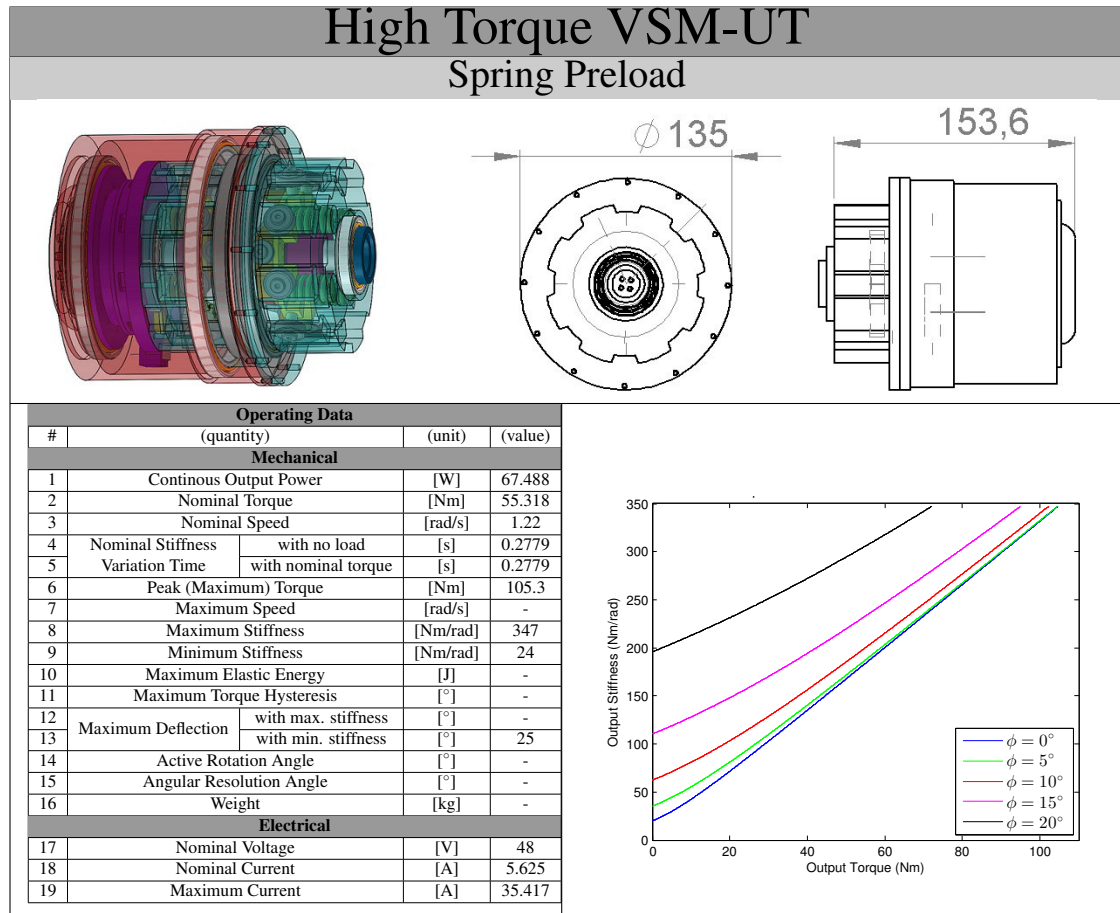


Table 4.1: Incomplete Datasheet of VSM Design

Chapter 5

Proof of Concept

Theoretically there is already a possible implementation with adapted requirements presented in the previous chapter. It is of importance however, that the theory of chapter 3.1 is validated by a proof of concept before purchasing rather expensive components like the 'TQ Robodrive', the 'Harmonic Drive' and the thin section bearings. Hence the adaptation of the design towards (rapid prototyping) usage of cheaper components and measurement equipment is the first part of this chapter. Later on the new design is tested accordingly.

5.1 Adaptation of Design/Rapid Prototyping

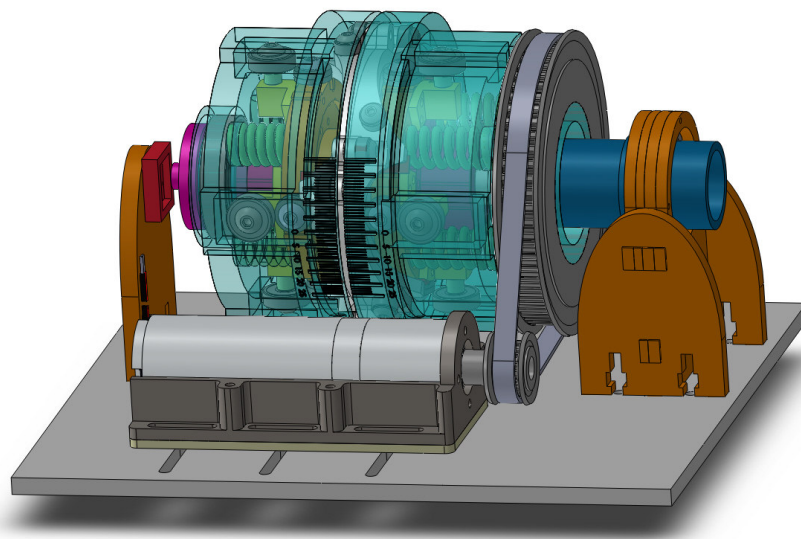


Figure 5.1: SOLIDWORKS Model of Test Setup

Most parts of the test setup are 3D-printed and laser-cut, therefore the spring force has to be decreased such that the plastic material does not crack. Therefore more

compliant springs, that are available in the RAM-group laboratory replace the Die Springs. The spring constant k had to be evaluated and was measured using a newton-meter and different weights. The Setup can be seen in Appendix A (fig.A.9) together with a plot of the measured Force vs Deflection (fig. A.10), resulting in a spring constant of $k = 0.7401 [N/mm]$.

Based on this Spring constant and the modeling of Output torque related to the state of spring explained in chapter 3.1 a Deflection vs Output torque plot for the test setup can be calculated. The spring used for the test setup has a free length of $l_f \approx 56 [mm]$, whereas the calculations for the cam profile were based on a spring with $l_f = 38.1 [mm]$. Regarding this aspect the state of spring has to be modified such that an initial compression of $56 - 38.1 [mm]$ is added. The results of the calculated Torque based on the state of spring s are shown below in fig. 5.2.

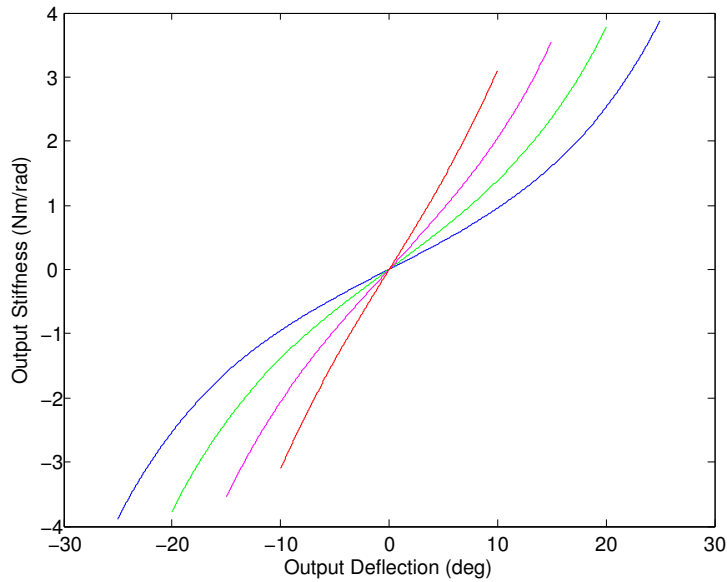


Figure 5.2: Deflection vs Output Torque for Springs used in Test Setup

The figure 5.1 depicts the test setup drawn in SOLIDWORKS, which was realized and tested. The main module of the VSA without the motor is only modified to a minimum extend. As mentioned before the springs are altered but also the 47mm 'Kaydon Reali-Slim mm metric Bearings' on the left and right side of the module are replaced by more bulky but cheaper bearings from misumi. To support the Rotational Cups angularly in the middle and still replace the more expensive 105mm thin section bearings, eight smaller bearings are attached to the support cup in rotational and radial direction. Concerning the motor, a 'maxon DC motor 326754' with 'maxon gear 166942' available in the RAM-laboratory was utilized. Instead of the 'Harmonic Drive' a belt pulley system was implemented, which can be ten-

sioned by adjusting the motor position on the base plate. One might notice that this test setup is back-drivable since no breaks are included in the model. One of the rotating cups was attached to the base plate together with the motor. This implies that the design is reversed for testing and the torque has to be applied to the main shaft instead of the rotating cups. Consequently the main shaft has to be kept in place by a bearing connected to the base plate (inside the orange connector on the rightmost side of fig.5.1). To obtain the Output torque τ_{out} a force/torque Sensor 'ATI mini 40' was used and the deflection angle φ was measured by a magnetic encoder 'AS5048A Rotary sensor' shown in picture

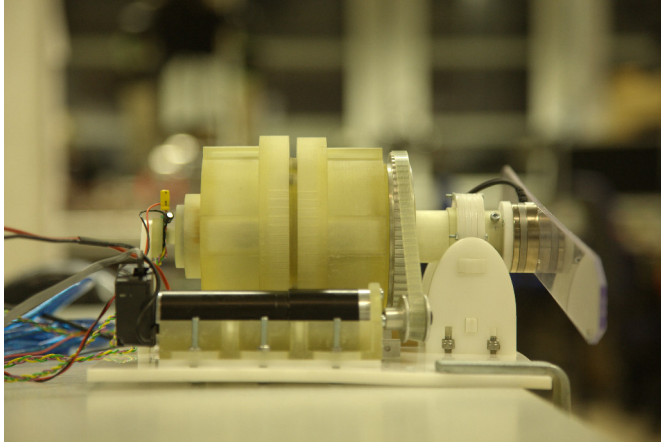


Figure 5.3: Fully Assembled Test Setup with F/T Sensor(right) and Magnetic Encoder(left).

5.3. Torque was applied by attaching a perspex bar to the torque sensor. The frame parts, such as the base plate, the part aligning the encoder with the main shaft and the parts that hold the main shaft on the right hand-side were laser-cut. The main shafts inside of the VSA-mechanism attached to the cam profiles were made out of aluminum by turning, because the linear bearing that centers the roller-base would impose friction if using plastic material. All other parts were 3D-printed. The data of the encoder was read by an 'Arduino Mega 2560' connected to a USB-port and the force/torque sensor by a Net Box connected through Ethernet. Capturing and processing was done by a 'Real-Time-Workshop Simulink' Model.

5.2 Test and Results

The goal of the testing is to show that the prototype behaves like expected or in other words that the plots of fig.5.2 are repeatable. Therefore the setup had to be tested for four different stiffness presets and the torque should be applied in a continual and non-disruptive manner. According to these criteria the measurements were carried out and resulted in the plots of hysteresis shown in fig. 5.4. Two hysteresis loops ranging from minimum to maximum possible deflection angle are plotted for each stiffness preset.

From the results different conclusions can be drawn. First of all one can obtain that for each stiffness preset the hysteresis loop has smaller ranges of deflection - so a

diagonal through the minimum and maximum values for deflection and torque will have a steeper slope for increasing stiffness presets - resulting in higher stiffnesses for higher stiffness presets. So in that concern the Prototype behaves like expected. Though the shape of each loop is not entirely smooth, the progressive shape of each loop is the same as in the expected plots. On top of that the maximum and minimum Output torque values seem to respond to the expected plots, except for the torque values of the green curve ($\phi = 5^\circ$), which overshoot by a small amount.

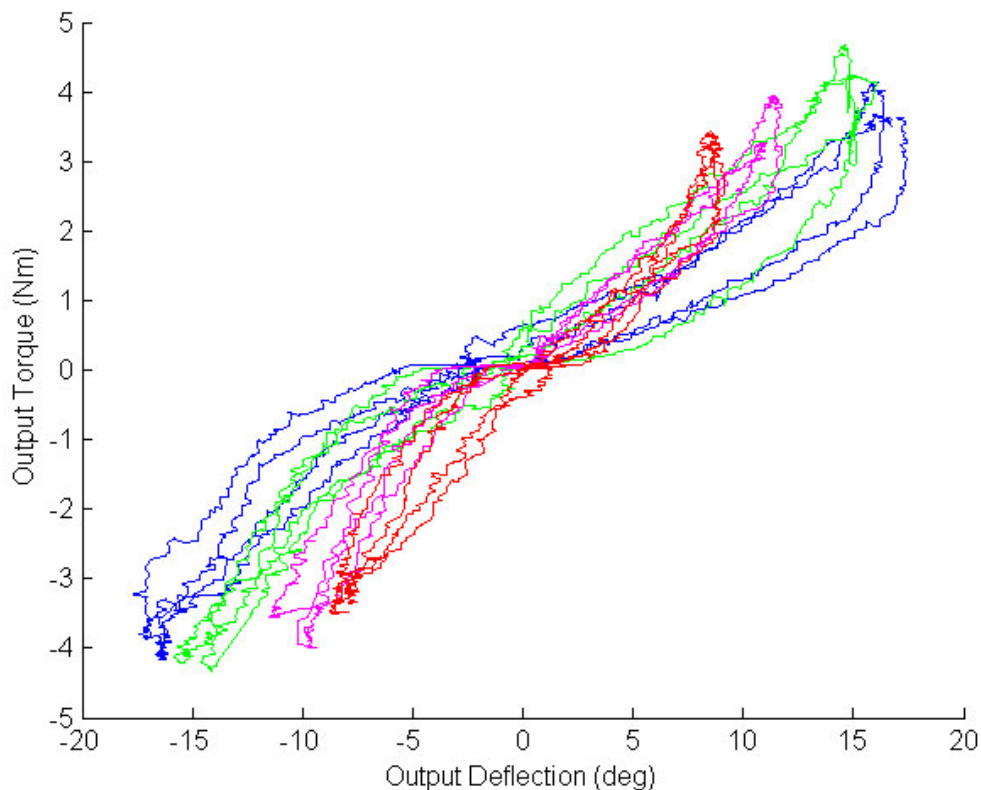


Figure 5.4: Deflection vs Output Torque obtained by testing

Regarding the aspects in which the test setup did not perform as presumed it is clear that there are some issues with the minimum and maximum deflection angles compared to the calculated values. For the stiffest setting of $\phi = 15^\circ$ or the red curve in the figure 5.4 the range should be from $\phi = -10^\circ$ to $\phi = 10^\circ$ and it actually is $\phi \approx [-8.8^\circ \ 8.8^\circ]$. Which is still reasonable regarding the friction in the test setup. For $\phi = 0$ and an assumed range of $[-25^\circ \ 25^\circ]$, the measured deflections however range from $\phi \approx -17.2^\circ$ to 17.2° . During the test of the prototype play and slip of the rollers on the cam-profile around zero deflection was detected and decreased for higher stiffness presets and was measured for the most compliant setting by rotating the main shaft without applying a torque to the system. In the discussion an attempt was made to tune the plot according to the measured angle of distortion or play.

Chapter 6

Discussion

The dimensions of the design realization of chapter 4 are not within the limits of the adapted requirements of 130[mm] in length and 150[mm] in diameter. However if integrated properly into the DD, a length of 150[mm] can probably be achieved when rearranging some components on the interface. In any case the requirements are already altered towards a rather large Variable Stiffness Joint compared with the models the VSM is based on ('VS-Joint' and 'FSJ'). A reason for this could be the necessary connection between the two joint motors of the differential drive, which is not a part of the existing VS models. A possible solution towards a more compact variable stiffness actuator could be to reconsider the implemented springs. In the fig. 4.1 it can be observed that there is some space lost next to the linear guidance on both sides of the rollerbase. This space can probably be used more efficiently if integrating more but shorter springs in a closed circle around the shaft. This could lead to a shorter VS-mechanism and would make room for the big motor and gear system. On the other hand the mechanism is quite complex and redesigning will take some time, that could also be spent investigating on a new high torque variable stiffness actuator based on for example the lever arm mechanism. Contrarily, the progressive torque-deflection behavior of the adapted VS-principle is leading to benefits in the maximum torque characteristics for a broader range in stiffness settings compared to the lever arm mechanism.

Additional time has to be spent on the testing of the clutches, because only three out of the 10 tests of differently configured clutches were actually self locking in [17]. An alternative to this could be the use of a worm gearbox which would be feasible if the entire mechanism is more compact.

The tests of the prototype showed, that the measured torque corresponds with the modeled expectations and an Output torque of 100[Nm] could be reached for the real design. For the deflection of the joint on the contrary was observed that a rapid prototype is not a solution. The shift in deflection due to slipping of the bearings on the 3D printed plastic material can be detected in fig.5.4. For zero torque there

is still some deflection at hand. During the test these measurement errors were encountered by trying to collect less data points at zero torque, which did not work out entirely. An attempt to make up for these errors by measuring the total shift in deflection for zero torque and zero stiffness preset and including it into the plot is made in fig. 6.1 below.

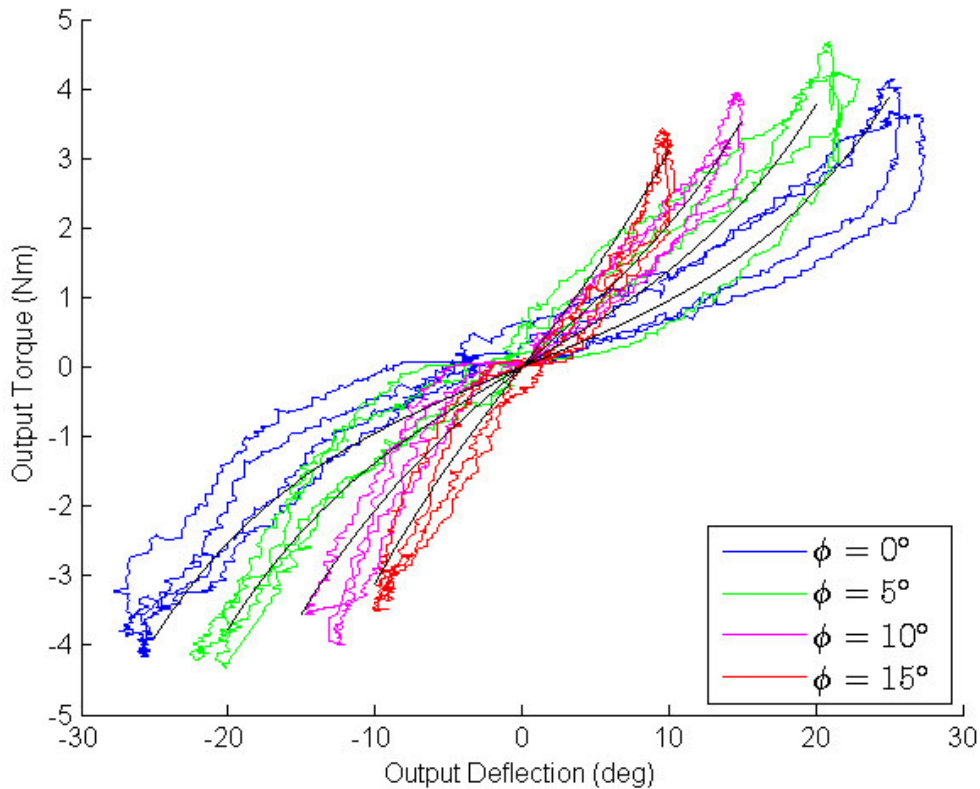


Figure 6.1: Compensated Deflection vs Output Torque Plot. The expected plots are depicted in black colour.

For the zero stiffness preset half of the range (a factor 1.571) is taken as a gain for the deflection angle. For all following plots the gain was set to decrease by $\frac{1}{4}$, so that for the stiffest setup the gain is only a fourth of the initial gain. Now the plots are really close to the expected deflection behavior (black lines). The method is more cheating to get the right plots rather than a solution. However considering the decrease in error it could be argued, that the force that presses the rollers against the cam profiles increases with increasing stiffness presets and subsequently the rollers rather stay in place than slip off the profiles. Anyway this has to be considered an unproved theory and not a fact. Lastly, it has to be mentioned that the motor in the test setup could not withstand the applied torque. Hence, a non-back-drivable module is a requisite for this Variable Stiffness Actuator.

Chapter 7

Conclusion and Future Work

7.1 Conclusion

The report presents a possible 'High-Torque VSM' solution for the Differential Drive. Possible is the key word, because the VSM design would have to be adapted to fit into the DD and the components are expensive as well as not mainly off-shelf. The High-Torque task was fulfilled at the expense of a complex mechanism and design.

The Tests resulted in anticipated performance and validate the concept except for the deflection characteristics. The two hysteresis plots for each stiffness preset on top of each other show that the measurements are repeatable and the joint behaves in an adequate manner even though the tests were executed with a rapid prototype. Altogether this work emphasizes on the antagonistic aspects of the high torque and compactness requirements. Achievements of one and the other is still an obstacle, but not impossible.

7.2 Future Work

- Possible recalculation of Spring setup for a more compact actuator
- Replacing roller (bearing plus shoulder bolt) by actual cam rollers
- Adjusting Rotor Axle and Stator Housing to be reusable
- FEM ANALYSIS of the mechanism, especially shaft, which is the most likely component that needs checking (only try-out done in SOLIDWORKS and not part of report)
- Research on self-locking breaks and testing of proposed breaks
- Research on torsional spring between rotating supports to shift equilibrium position and possibly lower the necessary motor-torque

Appendix A

A.1 Calculation of Leaf Spring

According to [19] the maximum deflection of a leaf spring can be described as:

$$\delta_{max} = \frac{4Fl^3}{Ebt^3} \quad (\text{A.1})$$

Where E is the modulus of elasticity taken as 180 [GPa] for stainless steel [20], l is the characteristic length of the spring, which was chosen to be 40 [mm], F is the applied force of $F = \frac{100000}{40} \frac{[Nmm]}{mm} = 2500N$, b is the width and t is the thickness. Interesting in this calculation is the relation of width and thickness, when setting the maximum deflection to $\delta_{max} = 10, 15[mm]$.

$$\text{For } \delta_{max} = 10 [mm] : \quad (\text{A.2})$$

$$bt^3 = 355.56[mm^4] \quad (\text{A.3})$$

$$\text{For } \delta_{max} = 15 [mm] : \quad (\text{A.4})$$

$$bt^3 = 237.04[mm^4] \quad (\text{A.5})$$

Assuming that a maximum thickness of $t = 2[mm]$ the leaf spring would still be compliant without occurrence of permanent deformation, the width is $b = 44.44 [mm]$ and $b = 29.63 [mm]$ for $\delta_{max} = 10, 15 [mm]$ respectively.

A.2 Calculation of Pivot Point Dimension for Lever Arm Mechanism

The shear force acting on the pivot pin can be calculated by the following equation from [21].

$$\tau_{USS} = \frac{2F}{\pi d^2} \quad (\text{A.6})$$

In this equation τ_{USS} is the ultimate shear stress, F the applied force and d the diameter of the pin, which we are interested in. The ultimate shear stress can be obtained by evaluating $\tau_{USS} \approx 0.75\tau_{UTS}$ due to [22], with $\tau_{UTS} = 860$ [MPa] ([20]). The torque-deflection plot of the 'vsaUT-II' in [8], shows that for the smallest deflection the biggest Output torque is achieved. So it can be assumed that the pin is close to the Output. If the complete lever arm would be $10[cm]$, it is assumed that the distance between the Output and pin would be approximately $1[cm]$ to withstand a torque of $100[Nm]$. This results in a force of $F = \frac{100[Nm]}{0.01[m]} = 10000[N]$. Plugging all the values into the equation results in a pin diameter of:

$$d = \sqrt{\frac{2F}{0.75\tau_{UTS}\pi}} = 3.1417[mm] \quad (A.7)$$

A.3 MATLAB

```

%CALCULATION FOR DIFFERENT SPRINGS SETUPS
%
%DEFLECTION RANGE: defl =[-15 15]deg =[-15 15]*pi/180 rad ~ [-0.26 0.26]rad
%S_0 = 3.1
%-----
% SINGLE SPRING
% k = 144.45;
% l_f = 38.1, l_s = 28.194 -> s_max = 9.906 at defl = 0.2618;
% s = 3.1*exp(b*defl), inserting P(0.26,s_max) -> b = 4.4375,
% so s = 3.1*exp(4.375*defl)
% tcam = k*b*(S_0^2)*exp(2*b*(defl+theta)) =6159.98*exp(8.875*(defl+theta))
defl = [-0.26:0.0001:0.26];
theta = 0;
tcup = (6.15998e+03)*exp(8.875*(defl+theta));
tcdown = (6.15998e+03)*exp(8.875*(-defl+theta));
tot = tcup - tcdown;
figure(11),clf;
b = plot(180/pi*defl,0.001*tot); %0.001 to convert from mm to m
hold on;

defl = [-0.21:0.0001:0.21];
theta = 0.05;
tcup = (6.15998e+03)*exp(8.875*(defl+theta));
tcdown = (6.15998e+03)*exp(8.875*(-defl+theta));
tot = tcup - tcdown;
plot(180/pi*defl,0.001*tot);

defl = [-0.16:0.0001:0.16];
theta = 0.1;
tcup = (6.15998e+03)*exp(8.875*(defl+theta));
tcdown = (6.15998e+03)*exp(8.875*(-defl+theta));
tot = tcup - tcdown;
plot(180/pi*defl,0.001*tot);

```

Figure A.1: Torque-Deflection MATLAB file for different Spring Setups, Page 1.

```

%-----
% SPRINGS IN PARALLEL
% ktot = 190.48;
% l_f = 38.1, l_s = 25.145-> s_max = 12.995 at defl = 0.2618;
% s = 3.1*exp(b*defl), inserting P(0.26,s_max) -> b = 5.4743,
% so s = 3.1*exp(5.4743*defl)
% tcam = k*b*(S_0^2)*exp(2*b*(defl+theta)) =10020.74*exp(10.948*(defl+theta))
defl = [-0.26:0.0001:0.26];
theta = 0;
tcup = (10.02074e+03)*exp(10.948*(defl+theta));
tcdown = (10.02074e+03)*exp(10.948*(-defl+theta));
tot = tcup - tcdown;
g = plot(180/pi*defl,0.001*tot,'green');

defl = [-0.21:0.0001:0.21];
theta = 0.05;
tcup = (10.02074e+03)*exp(10.948*(defl+theta));
tcdown = (10.02074e+03)*exp(10.948*(-defl+theta));
tot = tcup - tcdown;
plot(180/pi*defl,0.001*tot,'green');

defl = [-0.16:0.0001:0.16];
theta = 0.1;
tcup = (10.02074e+03)*exp(10.948*(defl+theta));
tcdown = (10.02074e+03)*exp(10.948*(-defl+theta));
tot = tcup - tcdown;
plot(180/pi*defl,0.001*tot,'green');

y1 = get(gca,'YLabel');
set(y1,'Interpreter','latex','string','$\tau_{ext}(Nm)$','fontSize',15,'fontWeight','demi')
set(y1,'Position',get(y1,'Position') - [0.2 -7 0])
set(y1,'Rotation',0.0)

```

PRO version Are you a developer? Try out the [HTML to PDF API](#)

pdfcrowd.com

Figure A.2: Torque-Deflection MATLAB file for different Spring Setups, Page 2.

```

x1 = get(gca,'XLabel');
set(x1,'Interpreter','latex','string','$\varphi(deg)$','fontSize',15,'fontWeight','demi')

set(b,'DisplayName','Single-Spring')
set(g,'DisplayName','Four-Springs-in-Parallel')
hl=legend([b,g],'location','southeast');
set(hl,'Interpreter','latex','fontSize',15,'fontWeight','bold')

```

Figure A.3: Torque-Deflection MATLAB file for different Spring Setups, Page 3.

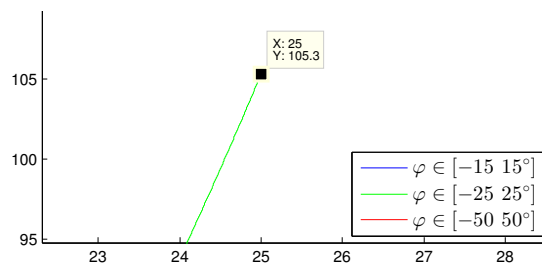


Figure A.4: Zoom into fig.3.4: Output torque at a deflection of 25°

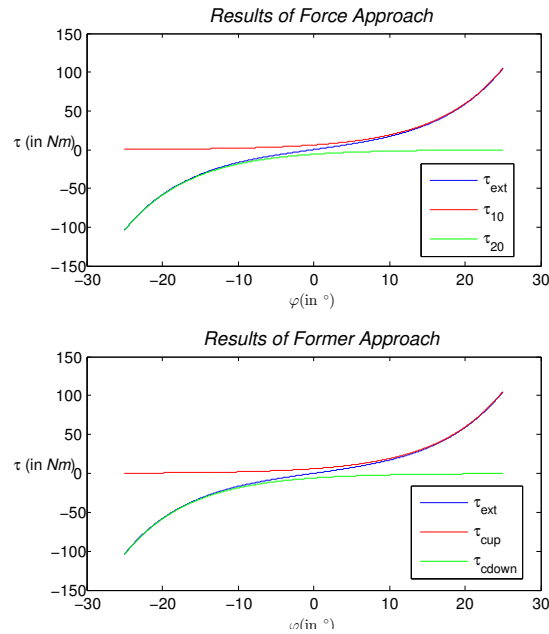


Figure A.5: Plots of force approach and approach based on [15]. Plotted with a deflection range of $\varphi = [-25^\circ \ 25^\circ]$ and $\phi = 0^\circ$. τ_{10} and τ_{cup} is the torque produced by the springs on the upper cam profile. τ_{20} and τ_{cdown} is the torque produced by the springs on the lower cam profile.

```

clc;
clear all;

k = 190.25;
%x=[-10.472:0.001:10.472]; %phi = x/r , with r = 40

x = sym('x');
y = sym('y');

for a = 1:1225
    %upper cam
    xar(a) = 180/pi * (-17.5+a/(35))/40;
    v = -17.5+a/(35);
    u = 3.1*exp(3.2775/40*x); %@(x)
    du = diff(u);
    mu = subs(du,x,v);
    alphau = atan(mu);

    Fsu = (subs(u,x,v))*k;
    Fnu = 1/cos(alphau)*Fsu;%
    F10 = sin(alphau)*Fnu; %mu*Fsu;
    Fsua(a) = double(Fsu);
    Fnua(a) = double(Fnu);
    F10a(a) = double(F10);
    t10(a) = double(F10).*0.04;

    %lower cam
    l = 3.1*exp(-3.2775/40*y); %@(y)
    dl = diff(l);
    ml = subs(dl,y,v);
    alpha1 = atan(ml);

```

Figure A.6: Torque-Deflection MATLAB file for fundamental approach comparison, Page 1.

```

Fsl = (subs(1,y,v))*k;
Fn1 = 1/cos(alpha1)*Fsl;
F20 = sin(alpha1)*Fn1;
F20a(a)= double(F20);
t20(a) = double(F20).*0.04;

Fext = F10+F20;
Text = 0.040.*Fext;
txt(a) = double(Text);
end
figure(11);clf;
plot(xar,F10a);
hold on;
plot(xar,F20a);

y1 = get(gca,'YLabel');

ylabel('F(N)')

set(y1,'Position',get(y1,'Position') - [0])

set(y1,'Rotation',0.0)

x1 = get(gca,'XLabel');
set(x1,'Interpreter','latex','string','$\varphi$')
title('\it(Resulting Forces of Cams)','FontSize',12)

fig1 = figure(21);clf;
set(fig1,'Position',[600 250 600 700])
subplot(2,1,1);
plot(xar,txt);
hold on;
plot(xar,t10,'red');
plot(xar,t20,'green');

```

PRO version Are you a developer? Try out the [HTML to PDF API](#)

pdfcrowd.com

Figure A.7: Torque-Deflection MATLAB file for fundamental approach comparison, Page 2.

```

y1 = get(gca,'YLabel');

ylabel('\tau (in \itNm)')

set(y1,'Position',get(y1,'Position') - [0])

set(y1,'Rotation',0.0)

x1 = get(gca,'XLabel');
set(x1,'Interpreter','latex','string','$\varphi$')
title('\it(Results of Force Approach)','FontSize',12)
legend('\tau_{ext}','\tau_{1_0}','\tau_{2_0}',[290,0,1,580]);

def1 = [-0.43633:0.0001:0.43633];
theta = 0;
tcup = (5.9995e+03)*exp(6.55504*(def1+theta));
tcdown = -(5.9995e+03)*exp(6.55504*(-def1+theta));
tot = (tcup + tcdown);
subplot(2,1,2);
plot(180/pi *def1,0.001*tot);
hold on;
plot(180/pi *def1,0.001*tcup,'red');
plot(180/pi *def1,0.001*tcdown,'green');

y1 = get(gca,'YLabel');
x1 = get(gca,'XLabel');

ylabel('\tau (in \itNm)')

set(y1,'Position',get(y1,'Position') - [0])

set(y1,'Rotation',0.0)

set(x1,'Interpreter','latex','string','$\varphi$')
legend('\tau_{e_x_t}','\tau_{cup}','\tau_{cdown}',[290,0,0,170]);

```

PRO version Are you a developer? Try out the [HTML to PDF API](#)

pdfcrowd.com

Figure A.8: Torque-Deflection MATLAB file for fundamental approach comparison, Page 3.



Figure A.9: Setup for the measurement of the Spring constant k including Newton-meter, weights(below) and scale.

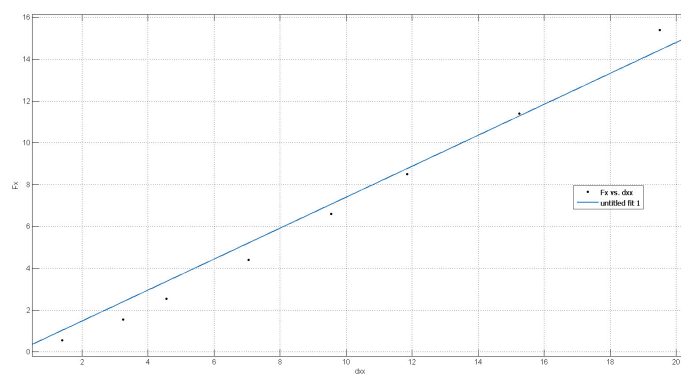


Figure A.10: Plot of Measured Spring Deflection vs Measured Force. The Data was evaluated using Matlab Curve Fitting with $F = kx$ and resulted in $k = 0.7401$ [N/mm].

Appendix B

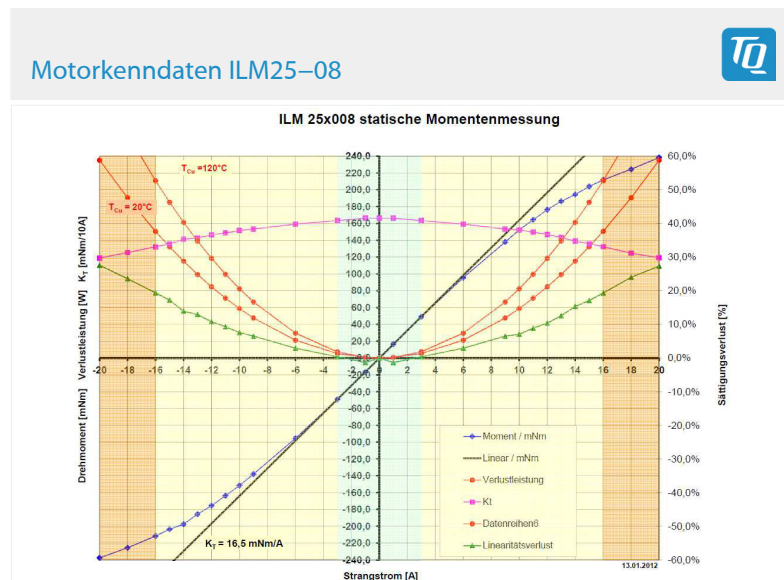


Figure B.1: Characteristic data of TQ Drive ILM25x08.

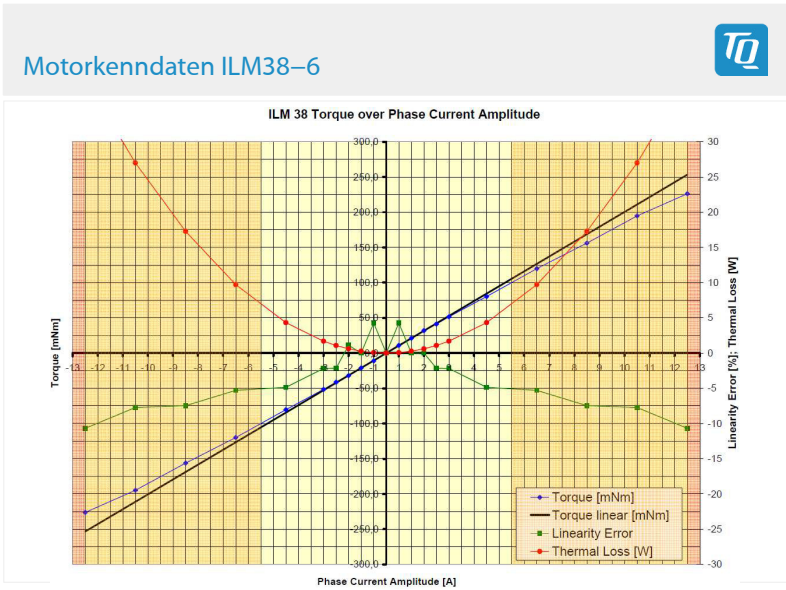


Figure B.2: Characteristic Data of TQ Drive ILM38x06.

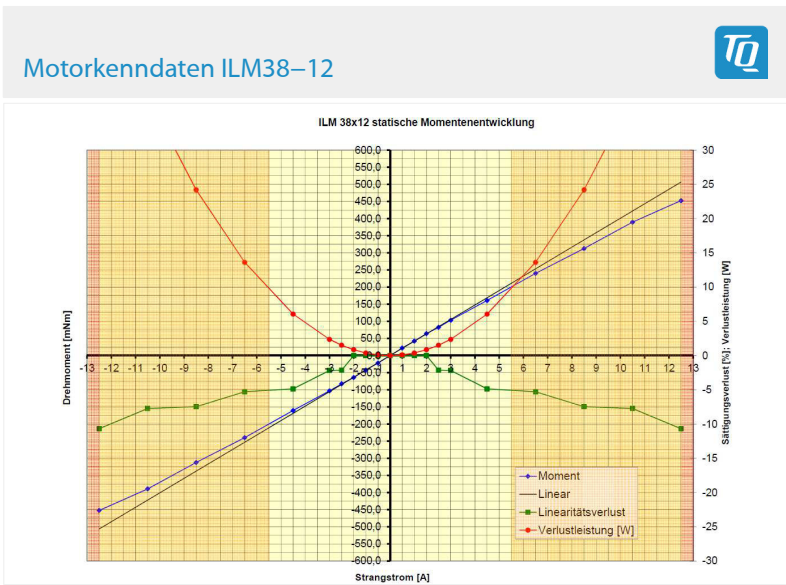


Figure B.3: Characteristic Data of TQ Drive ILM38x12.

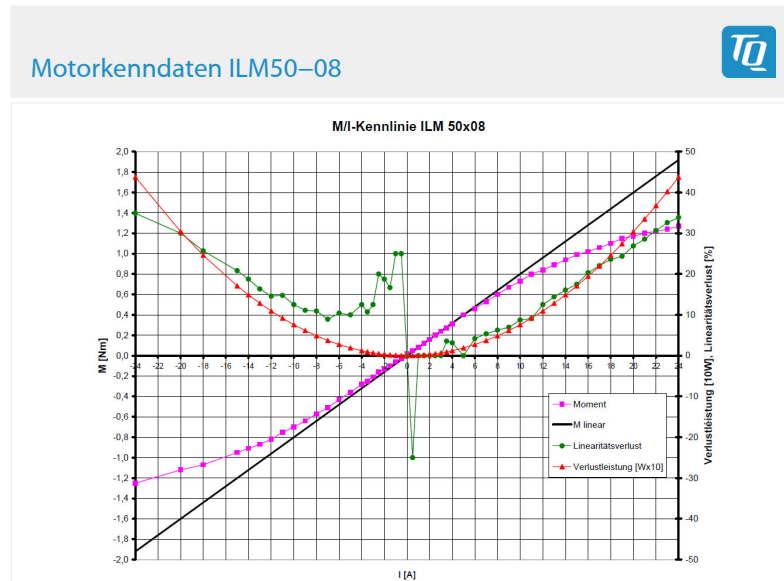


Figure B.4: Characteristic Data of TQ Drive ILM50x08.

Bibliography

- [1] S. S. Groothuis, S. Stramigioli and R. Carloni
Towards Novel Assistive Robotic Arms: a survey of the present and an outlook on the future
IEEE Robotics and Automation Magazine, 2013.
- [2] SHERPA PROJECT
<http://www.sherpa-project.eu/sherpa/>
Integrated Project IP #600958, supported by the European Community under the 7th Framework Programme, (01/02/2013 – 31/01/2017).
- [3] M. Fumagalli, S. Stramigioli and R. Carloni
Analysis of the Dynamics of a Variable Stiffness Differential Drive (VSDD)
Funded by the European Commission's Seventh Framework Programme as part of the project SHERPA.
- [4] B. Vanderborght, A. Albu-Schaeffer, A. Bicchi, E. Burdet, D.G. Caldwell, R. Carloni, M. Catalano, O. Eiberger, W. Friedl, G. Ganeshd, M. Garabini, M. Grebenstein, G. Grioli, S. Haddadina, H. Hoppnera, A. Jafari, M. Laffranchi, D. Lefeber, F. Petit, S. Stramigioli, N. Tsagarakis, M. Van Damme, R. Van Ham, L.C. Visser, S. Wolf
Variable impedance actuators: A review
Elsevier B.V., Robotics and Autonomous Systems, 2013.
- [5] K. W. Hollander, T. G. Sugar and D. E. Herring
Adjustable Robotic Tendon using a 'Jack Spring'
Proc. IEEE, 9th International Conference on Rehabilitation Robotics, 2005.
- [6] J. Choi, S. Hong, W. Lee, and S. Kang
A Variable Stiffness Joint using Leaf Springs for Robot Manipulators
IEEE, International Conference on Robotics and Automation, Kobe, Japan, 2009.
- [7] T. Morita and S. Sugano
Design and Development of a new Robot Joint using a Mechanical Impedance

- Adjuster*
IEEE, International Conference on Robotics and Automation, Tokyo, Japan, 1995.
- [8] S. S. Groothuis, G. Rusticelli, A. Zucchelli, S. Stramigioli and R. Carloni
The Variable Stiffness Actuator vsaUT-II: Mechanical Design, Modeling, and Identification
IEEE/ASME: TRANSACTIONS ON MECHATRONICS, VOL. 19, NO.2, APRIL 2014.
- [9] M. Fumagalli, E. Barrett, S. Stramigioli, and R. Carloni
The mVSA-UT: a Miniaturized Differential Mechanism for a Continuous Rotational Variable Stiffness Actuator
IEEE RAS/EMBS, 4th International Conference on Biomedical Robotics and Biomechatronics, Roma, Italy. June 24-27,2012.
- [10] A. Jafari, N. G. Tsagarakis, B. Vanderborght and D. G. Caldwell
A novel Actuator with Adjustable Stiffness (AwAS)
IEEE/RSJ, International Conference on Intelligent Robots and Systems, Taipei, Taiwan, 2010.
- [11] A. Jafari, N. G. Tsagarakis and D. G. Caldwell
AwAS-II: A New Actuator with Adjustable Stiffness based on the Novel Principle of Adaptable Pivot point and Variable Lever ratio
IEEE, International Conference on Robotics and Automation, Shanghai, China, 2011.
- [12] S. Wolf and G. Hirzinger
A New Variable Stiffness Design: Matching Requirements of the Next Robot Generation
IEEE, International Conference on Robotics and Automation, Pasadena, USA, 2008.
- [13] B. Vanderborght, N. G. Tsagarakis, C. Semini, R. Van Ham and D. G. Caldwell
MACCEPA 2.0: Adjustable Compliant Actuator with Stiffening Characteristic for Energy Efficient Hopping
IEEE, International Conference on Robotics and Automation, Kobe, Japan, 2009.
- [14] S. Wolf, O. Eiberger and G. Hirzinger
The DLR FSJ: Energy based design of a variable stiffness joint

- IEEE, International Conference on Robotics and Automation, Shanghai, China, 2011.
- [15] L. C. Visser, R. Carloni and S. Stramigioli
Energy Efficient Variable Stiffness Actuators
Preprint submitted to IEEE Transactions on Robotics, 2011.
- [16] K.- H. Grote and J. Feldhusen
DUBBEL TASCHENBUCH FÜR DEN MASCHINENBAU
Springer, 21st Edition, P. G125, 2005.
- [17] B. Peerdeman, G. J. Pieterse, S. Stramigioli, H. Rietman, E. Hekman, D. Brouwery, and S. Misra
Design of Joint Locks for Underactuated Fingers
IEEE RAS and EMBS, 4th International Conference on Biomedical Robotics and Biomechatronics (BioRob), 2012.
- [18] G. Grioli, S. Wolf, M. Grabini, M. Catalano, E. Burdet, D. Caldwell, R. Carloni, W. Friedl, M. Grebenstein, M. Laffranchi, D. Lefeber, S. Stramigioli, N. Tsagarakis, M. van Damme, B. Vanderborght, A. Albu-Schaeffer and A. Bicchi
Variable Stiffness Actuators: the user's point of view.
VIATORS Specific Targeted Research Project, funded by the European Community under Contract IST-231554-2008, and by UE project SAPHARI ICT-287513.
- [19] K.- H. Grote and J. Feldhusen
DUBBEL TASCHENBUCH FÜR DEN MASCHINENBAU
Springer, 21st Edition, P. G55 (Blattfeder), 2005.
- [20] The Engineering Toolbox
http://www.engineeringtoolbox.com/young-modulus-d_417.html
- [21] K.- H. Grote and J. Feldhusen
DUBBEL TASCHENBUCH FÜR DEN MASCHINENBAU
Springer, 21st Edition, P. G35 (Bolzenverbindungen), 2005.
- [22] R. Beardmore
http://www.roymech.co.uk/Useful_Tables/Matter/shear_tensile.htm
Last updated: 23.03.2010.

Component References

- [23] Lee Spring Company
http://www.leespring.com/int_learn_hefty.asp
2014
- [24] LHL 750D 03, Lee Spring Company
http://www.leespring.com/uk_product_spec.asp?partnum=LHL750D03&springType=C&subType=H
2014, $k = 144.45N/mm$, $l_s = 38.1mm$, $l_s = 28.194mm$, $D_i n = 9.524mm$
- [25] LHL 625C 03, Lee Spring Company
http://www.leespring.com/uk_product_spec.asp?partnum=LHL625C03&springType=C&subType=H
2014, $k = 47.62N/mm$, $l_f = 38.1mm$, $l_s = 25.145mm$, $D_0 = 14.808mm$
- [26] TQ Group GmbH
<http://www.tq-group.com/produkte/produktdetail/prod/leichtbau-torque-servomotoren/extb/Main/>
Copyright 2014
- [27] HD-CSD-2A, Harmonic Drive AG
<http://harmonicdrive.de/produkte/index.php/einbausaeetze/csd-2a.html>
Copyright 2014
- [28] Small Deep Groove Ball Bearings - Double Shielded, B695ZZ(Rollers), B625ZZ(Guidance Bearings), MISUMI Corporation
<http://uk.misumi-ec.com/eu/ItemDetail/10300107560.html>
- [29] Low Head Shoulder Bolts, MISUMI Corporation
<http://uk.misumi-ec.com/eu/ItemDetail/10300248960.html>
- [30] Linear Bushings, LMUT 16, MISUMI Corporation
http://uk.misumi-ec.com/pdf/fa/pl_0277.pdf
- [31] Thin Section Bearings,'Reali-Slim MM metric bearings 8mm Type A-angular contact', K02508AR0, Kaydon Corporation Inc.
http://www.kaydonbearings.com/RealiSlim_metric_bearings_8mm_typeA.htm
2010-2014

- [32] Thin Section Bearings,'Reali-Slim MM metric bearings 8mm Type A-angular contact', K09008AR0, Kaydon Corporation Inc.
http://www.kaydonbearings.com/RealiSlim_metric_bearings_8mm_typeA.htm
2010-2014
- [33] Rillenkugellager, offene Ausf¼hrung, SB6704ZZ(Carrier Bearings), MIS-UMI Corporation
<http://de.misumi-ec.com/eu/ItemDetail/10300115350.html>
- [34] Deep Grove Ball Bearings - Double Shielded, SB6703ZZ(Carrier Bearings), MISUMI Corporation
<http://uk.misumi-ec.com/eu/ItemDetail/10302272750.html>
- [35] Thin Section Bearings,'Reali-Slim MM metric bearings 8mm Type A-angular contact', K11008AR0, Kaydon Corporation Inc.
http://www.kaydonbearings.com/RealiSlim_metric_bearings_8mm_typeA.htm
2010-2014
- [36] Thin Section Bearings, CSCAA017-TV, Schaeffler/medias professional
http://medias.schaeffler.de/medias/en!hp.ec.br.pr/CSCAA.-TV*CSCAA017-TV
- [37] Push and Pull Solenoid, 110C, Geeplus
http://www.geeplus.biz/FTPROOT/small_push_pull_solenoid_110.pdf
08/2011